Supplement of Earth Syst. Sci. Data, 16, 4995–5007, 2024
https://doi.org/10.5194/essd-16-4995-2024-supplement

Open Access Earth System Science Data

Supplement of

Large synthesis of in situ field measurements of the size distribution of mineral dust aerosols across their life cycles

Paola Formenti and Claudia Di Biagio

Correspondence to: Paola Formenti (paola.formenti@lisa.ipsl.fr) and Claudia Di Biagio (claudia.dibiagio@lisa.ipsl.fr)

Table S1. Listing of the observations contributing to the in situ dataset. Summary of available field studies data from past field campaigns. Data are categorized as SOURCE (emission and <1 days of transport), MRT or Mid−Range Transport (1 to 4 days of transport), and LRT or Long−Range Transport (> 4 days of transport), respectively. Data are ordered chronologically. In the Table the "Diameter measured" column indicates the diameter definition from the used technique. For data for which multiple instruments are used to measure the size distribution the "Diameter measured" column indicate the assumed dominant diameter definition in the considered study, usually corresponding to the technique documenting the majority of the dust size range. The "Diameter size data" column provides instead the diameter definition as reported in the size distribution data from the original paper. In this column "geometrical" means that corrections are applied in the original paper to convert the measured diameter (projected area, aerodynamic, optical) into a geometrical diameter. More details on the description of each dataset and on the different diameter definitions and their conversions to geometrical (volume−equivalent, sphere assumption) diameter are provided in Texts S3 and S4, respectively. Acronyms for the field campaign and the different instruments are reported in Texts S1 and S2, respectively.

Table S2. Geographical coordinates of datasets shown in Figure 1.

Table S3. Synthesis of diameter definitions and corrections under spherical and aspherical assumptions.

Figure S1. Aspherical to spherical ratio (ASR(D_{geom})) obtained at 1.53−0.0032i refractive index for different OPC models as retrieved from calculations in Formenti et al. (2021) (CDP, FSSP−300, GRIMM1.109/1.129, PCASP) and at 1.48−0.0012i and 1.51.0038i as calculated in Huang et al. (2021) (CLIMET, WELAS) assuming tri−axial ellipsoids dust. The yellow dotted curve represents the average curve obtained by averaging the different datasets as explained in the text, smoothed over a 10−width running mean window.

Figure S2. Comparison of SOURCE, MRT, and LRT data for LEV1 (top), LEV2a (center), and LEV2b (bottom) analysis. As in Fig. 3 in the main manuscript, all datasets reported in this figure are normalized at the integral of 1 in the common diameter range 0.35 to 17.8 µm and shown as mean ± standard deviation.

Figure S3. Vertical distribution of the different datasets used in the present analysis for the SOURCE (black), MRT (blue), and LRT (red).

Figure S4. Lognormal size distributions fitting the LEV2a and LEV2b mean values of the three SOURCE; MRT, and LRT dust categories. Parameters (total volume concentration, V_{tot} ($nm^3\ cm^{-3}$), volume median diameter, VMD (µm), geometric standard deviation, σ) for the log-normal modes are indicated in the figure.

Text S1. Acronyms and year of field campaigns

Text S2. Size instrumentation generalities and acronyms

Text S3. Conversion formulas between diameter definitions

Text S4. In situ dataset description

Table S1. Listing of the observations contributing to the in situ dataset. Summary of available field studies data from past field campaigns. Data are categorized as SOURCE (emission and <1 days of transport), MRT or Mid−Range Transport (1 to 4 days of transport), and LRT or Long−Range Transport (> 4 days of transport), respectively. Data are ordered chronologically. In the Table the "Diameter measured" column indicates the diameter definition from the used technique. For data for which multiple instruments are used to measure the size distribution the "Diameter measured" column indicate the assumed dominant diameter definition in the considered study, usually corresponding to the technique documenting the majority of the dust size range. The "Diameter size data" column provides instead the diameter definition as reported in the size distribution data from the original paper. In this column "geometrical" means that corrections are applied in the original paper to convert the measured diameter (projected area, aerodynamic, optical) into a geometrical diameter. More details on the description of each dataset and on the different diameter definitions and their conversions to geometrical (volume−equivalent, sphere assumption) diameter are provided in Texts S3 and S4, respectively. Acronyms for the field campaign and the different instruments are reported in Texts S1 and S2, respectively.

Reference	Ground/Airborne, location, field campaign acronym	Measurement technique	Diameter measured	Diameter size data	Source	MRT	LRT
Gillette et al. (1972, 1974) Gillette (1974)	Ground, Texas and Nebraska	Microscopy	Projected−area	Projected−area	X		
Schütz (1981)	Ship−based, Atlantic Ocean	Microscopy	Projected−area	Projected−area		X	
	Ship−based, Atlantic Ocean						X
d'Almeida (1987)	Ground, Niger	Microscopy	Projected−area	Projected−area		X	
de Reus et al. (2000)	Airborne, Tenerife – Canary Islands, ACE2	DMPS + OPC	Optical	Geometrical		X	
Maring et al. (2000)	Ground, Izana – Canary Islands	SMPS + APS	Aerodynamic	Geometrical		X	
Formenti et al. (2001)	Ground – Brasil, CLAIRE	Chemical composition	Aerodynamic	Aerodynamic			X
Bates et al. (2002)	Ground, Indian Ocean, AEROSOLS99	DMPS+APS	Aerodynamic	Geometrical		X	
	Ground, Indian Ocean, INDOEX					X	
Maring et al. (2003)	Ground, Puerto Rico, PRIDE	SMPS+APS	Aerodynamic	Geometrical			X
Reid et al. (2003a)	Airborne, Puerto Rico, PRIDE	Microscopy	Projected−area	Projected−area			X
Reid et al. (2003b)	Airborne, Puerto Rico, PRIDE	OPC	Optical	Optical			X
	Ground, Puerto Rico, PRIDE	Chemical composition	Aerodynamic	Geometrical			X
Clarke et al. (2004)	Airborne, Sea of Japan, ACE−Asia & TRACE−P	OPC	Optical	Optical		X	
Fratini et al. (2007)	Ground, Gobi desert	OPC	Optical / aerodynamic**	Geometrical	X		
Kobayashi et al. (2007)	Ground, Japan	Coulter multisizer	Geometrical	Geometrical		X	
						X	
Otto et al. (2007)	Airborne, Cape Verde, ACE2	DMPS + OPC	Optical	Geometrical		X	
Chou et al. (2008)	Airborne, Niger, DABEX	Microscopy	Projected−area	Projected−area		X	
McConnell et al. (2008)	Airborne, Dakar, DODO1	OPC	Optical	Optical		X	
	Airborne, Dakar, DODO2					X	
Osborne et al. (2008)	Airborne, Niger, DABEX	OPC	Optical	Optical		X	
Rajot et al. (2008)	Ground, Niger, AMMA – Local erosion	OPC	Optical	Optical	X		
	Ground, Niger, AMMA – advection distant sources					X	
Reid et al. (2008)	Ground, Saudi Arabia, UAE2 – A	APS	Aerodynamic	Aerodynamic		X	
	Ground, Saudi Arabia, UAE2 – B					X	
Sow et al. (2009)	Ground, Niger, AMMA	OPC	Optical	Optical	X		
Wagner et al. (2009)	Airborne, Portugal, DARPO	OPC	Optical	Geometrical		X	
Weinzierl et al. (2009)	Airborne, Morocco, SAMUM1	OPC	Optical	Geometrical		X	
Müller et al. (2010)	Ground, Cape Verde, RHAMBLE	SMPS + APS	Aerodynamic	Geometrical		X	

Chen et al. (2011)	Airborne, Cape Verde/West Sahara, NAMMA	OPC + APS	Aerodynamic	Geometrical		X	
Formenti et al. (2011)	Airborne, Niger, AMMA – erosion	OPC	Optical	Geometrical		X	
	Airborne, Niger, AMMA – transport					X	
Johnson and Osborne (2011)	Airborne, West Sahara, GERBILS	OPC	Optical	Geometrical		X	
Kandler et al. (2011)	Ground, Cape Verde (Praia), SAMUM2	DMPS+APS+microscopy	Projected–area	Projected–area		X	
Shao et al. (2011)	Ground, Australia, JADE	OPC	Optical	Geometrical	X		
Weinzierl et al. (2011)	Airborne, Cape Verde, SAMUM2	OPC	Optical	Geometrical		X	
Jung et al. (2013)	Barbados, BACEX	OPC	Optical	Optical			X
Ryder et al. (2013a, 2013b)	Airborne, West Sahara and Canary Islands, FENNEC – fresh dust category	OPC + OAP	Optical	Geometrical	X		
	Airborne, West Sahara and Canary Islands, FENNEC – aged dust category					X	
	Airborne, West Sahara and Canary Islands, FENNEC – SAL dust category					X	
Rosenberg et al. (2014)	Airborne, central Sahara, FENNEC	OPC + OAP	Optical	Geometrical	X		
Meloni et al. (2015)	Airborne, Lampedusa, GAMARF	OPC	Optical	Optical		X	
Denjean et al. (2016a)	Ground, Puerto Rico, DUST–ATTACk	SMPS + OPC	Optical	Geometrical			X
Denjean et al. (2016b)	Airborne, Mediterranean sea, ChArMEx/ADRIMED	SMPS + OPC	Optical	Geometrical		X	
Struckmeier et al. (2016)	Ground, Rome, DIAPASON2013–2014	APS	Aerodynamic	Aerodynamic		X	
Weinzierl et al. (2017)	Airborne, Cape Verde, SALTRACE	CPC + OPC	Optical	Geometrical		X	
	Airborne, Barbados, SALTRACE						X
Moran Zuoloaga et al. (2018)	Ground, Amazonian forest, GoAMAZON	OPC	Optical	Optical			X
Renard et al. (2018)	Airborne, Mediterranean sea, ChArMEx/ADRIMED	OPC	Optical	Geometrical		X	
Ryder et al. (2018)	Airborne, Cape Verde, AER–D	OPC + OAP	Optical	Geometrical		X	
Huang et al. (2019)	Ground, California	OPC	Optical	Geometrical	X		
Khalfallah et al. (2020)	Ground, Dar Dhaoui, Tunisia, Wind–O–V's	OPC	Optical	Geometrical	X		
González–Flórez et al. (2023)	Ground, Morocco, FRAGMENT	OPC	Optical	Geometrical	X		

** for Fratini et al. (2007) we used the dataset as retrieved by Kok et al. (2017) who converted the dataset as aerodynamic diameter.

Table S2. Geographical coordinates of datasets shown in Figure 1.

Reference_dataset	Latitude	Longitude	Altitude(m agl)	Type
Gillette_et_al.(1972)	42.1	-102.87	6	SOURCE
Gillette(1974)	32.24	-101.47	6	SOURCE
Gillette_et_al.(1974)	32.24	-101.47	6	SOURCE
Fratini_et_al.(2007)	41.9	100.7	12	SOURCE
Rajot_et_al.(2008)	13.5	2.6	3	SOURCE
Sow_et_al.(2009)	13.5	2.6	6.1	SOURCE
Shao_et_al.(2011)	-33.85	142.74	3.5	SOURCE
Ryder_et_al.(2013)	24	-6	1500	SOURCE
Rosenberg_et_al.(2014)	23	-7	500	SOURCE
Huang_et_al(2019)	35	-120.6	6	SOURCE
Kalfallah_et_al.(2020)	33.3	10.78	4	SOURCE
Gonzales_Flores_et_al.(2023)	29.83	-5.87	3.5	SOURCE
Schutz(1981)-defined_by_me_as_1000km	15	-12	0	MRT
d'Almeida(1987)windcarrying	15	-13	50	MRT
Maring_2000	28.3	-16.5	2360	MRT
deReus_et_al.(2000)	28	-16	4000	MRT
Bates2002	-28	50	0	MRT
Clarke_et_al.(2004)	38.85	130	3000	MRT
Kobayashi(2007)	35	135	0	MRT
Otto_et_al.(2007)	27.5	-14	4100	MRT
Chou_et_al.(2008)	16.2	5.5	750	MRT
McConnell_et_al.(2008)DODO1	19.9	-12.5	2500	MRT
McConnell_et_al.(2008)DODO2	19.9	-12.5	1000	MRT
Osborne_et_al.(2008)	15.5	5	500	MRT
Rajot_et_al.(2008)	13.5	12.6	3	MRT
Reid_et_al.(2008)	24.7	54.65	0	MRT
Wagner_et_al.(2009)	38.6	-7.9	3245	MRT
Weinzierl_et_al.(2009)	31.26	-7.5	3000	MRT
Muller_et_al.(2010)	16.9	-24.9	10	MRT
Chen_et_al.(2011)	17	-23	2500	MRT
Formenti_et_al.(2011)	13.5	2.6	2500	MRT
Formenti_et_al.(2011)	13.5	2.6	2500	MRT
Weinzierl_et_al.(2009)	31.26	-7.5	3000	MRT
Johnson_and_Osborne(2011)	18	-16	3000	MRT
Kandler_et_al.(2011)	14.9	-23.5	4	MRT
Weinzierl_et_al.(2011)	14.9	-23.5	750	MRT
Ryder_et_al.SAL(2013)	28	-2	2500	MRT
Ryder_et_al.aged(2013)	28	-14	2500	MRT
Meloni_et_al.(2015)	35.5	12.6	1500	MRT
Denjean_et_al.(2016b)	38.6	6.3	4000	MRT
Struckmeier_et_al.(2016)	41.8	12.6	0	MRT
Weinzierl_et_al.(2017)	15	-23.6	2600	MRT

Ryder_et_al.(2018)	20	-20	2950	MRT
Renard_et_al.(2018)	39.88	4.25	3300	MRT
Schutz(1981)-defined_by_me_as_5000km	15	-50	0	LRT
Formenti_et_al.(2001)	-1.9	-59.4	0	LRT
Maring_et_al.(2003)	18.2	-65.6	10	LRT
Reid_et_al.(2003)a	18.2	-65.6	3000	LRT
Reid_et_al.(2003)b	18.2	-65.6	0	LRT
Reid_et_al.(2003)b	18.2	-65.6	0	LRT
Jung_et_al.(2013)	13.2	-59.5	2100	LRT
Denjean_et_al.(2016a)	18.4	-65.6	10	LRT
Weinzierl_et_al.(2017)	13.2	-59.5	2300	LRT
Moran_Zuloaga_et_al.(2018)	-2.13	-59	60	LRT
Solar_Village	24.906933	46.397286	0	AERONET
Nes_Ziona	31.9225	34.789167	0	AERONET
SEDE_BOKER	30.855	34.782222	0	AERONET
IMS-METU-ERDEMLI	36.565	34.255	0	AERONET
Lecce_University	40.335111	18.111389	0	AERONET
Rome_Tor_Vergata	41.83955	12.647333	0	AERONET
Toulon	43.135556	6.009444	0	AERONET
Tamanrasset_INM	22.79	5.53	0	AERONET
Lille	50.611667	3.141667	0	AERONET
Banizoumbou	13.54693	2.66519	0	AERONET
Barcelona	41.38925	2.11206	0	AERONET
Granada	37.164	-3.605	0	AERONET
Evora	38.567833	-7.9115	0	AERONET
Saada	31.62583	-8.15583	0	AERONET
Izana	28.30932	-16.49906	0	AERONET
Capo_Verde	16.7325	-22.935499	0	AERONET
Ragged_Point	13.16	-59.4	0	AERONET
Dalanzadgad	43.6	104.4	0	AERONET
Birdsville	-25.9	139.35	0	AERONET

Table S3. Synthesis of diameter definitions and corrections under spherical and aspherical assumptions.

Diameter definition (technique)	Correction under spherical assumption	Correction under aspherical assumption
Geometrical (i.e., coulter counter), D_{geom}	$D_{geom,sph} = D_{geom}$	$D_{geom,asph} = D_{geom}$
Projected–area (i.e., microscopy), D_{area}	$D_{geom,sph} = D_{area}$	$D_{geom,asph} = D_{area}/1.56$
Aerodynamic (i.e., APS or cascade impactor), D_{aerod}	$D_{geom,sph} = D_{aerod}/1.58$	$D_{geom,asph} = D_{aerod}/1.45$
Mobility (i.e., DMPD or SMPS), D_m	$D_{geom,sph} = D_m/1.0$	$D_{geom,asph} = D_m/1.19$
Optical (i.e., OPC), D_{opt}	$D_{geom,sph} = D_{opt}$ (Mie theory)	$D_{geom,asph} = D_{geom,sph} \cdot ASR(D_{geom,sph})$

Figure S1. Aspherical to spherical ratio (ASR(D_{geom})) obtained at 1.53−0.0032i refractive index for different OPC models as retrieved from calculations in Formenti et al. (2021) (CDP, FSSP−300, GRIMM1.109/1.129, PCASP) and at 1.48−0.0012i and 1.51.0038i as calculated in Huang et al. (2021) (CLIMET, WELAS) assuming tri−axial ellipsoids dust. The yellow dotted curve represents the average curve obtained by averaging the different datasets as explained in the text, smoothed over a 10−width running mean window.

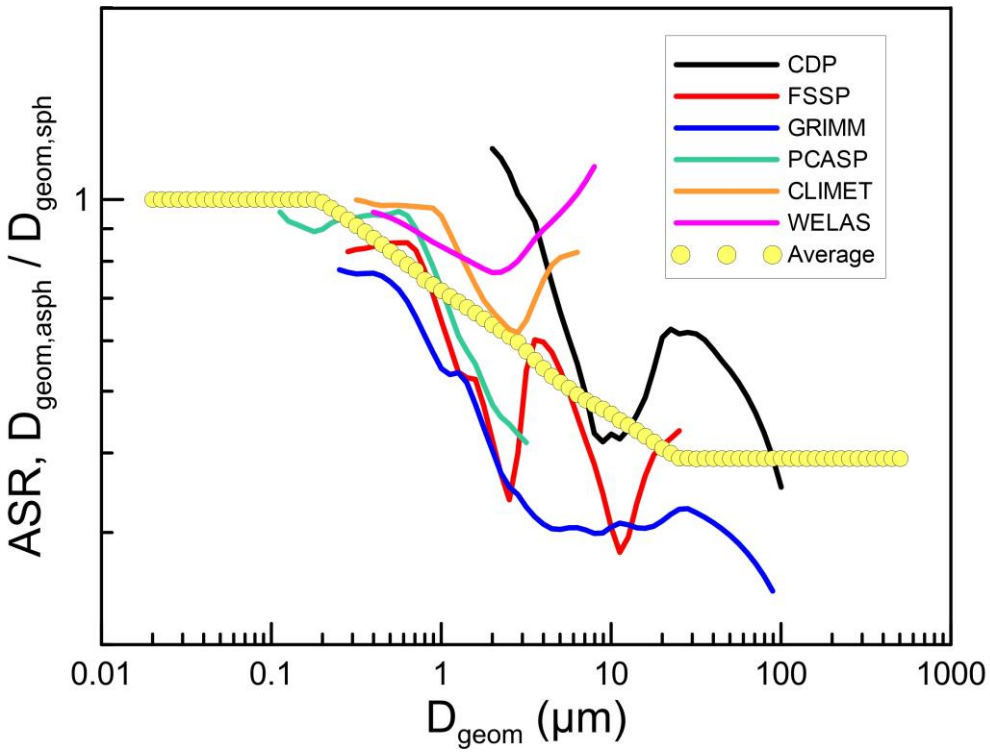

Figure S2. Comparison of SOURCE, MRT, and LRT data for LEV1 (top), LEV2a (center), and LEV2b (bottom) analysis. As in Fig. 3 in the main manuscript, all datasets reported in this figure are normalized at the integral of 1 in the common diameter range 0.35 to 17.8 µm and shown as mean ± standard deviation.

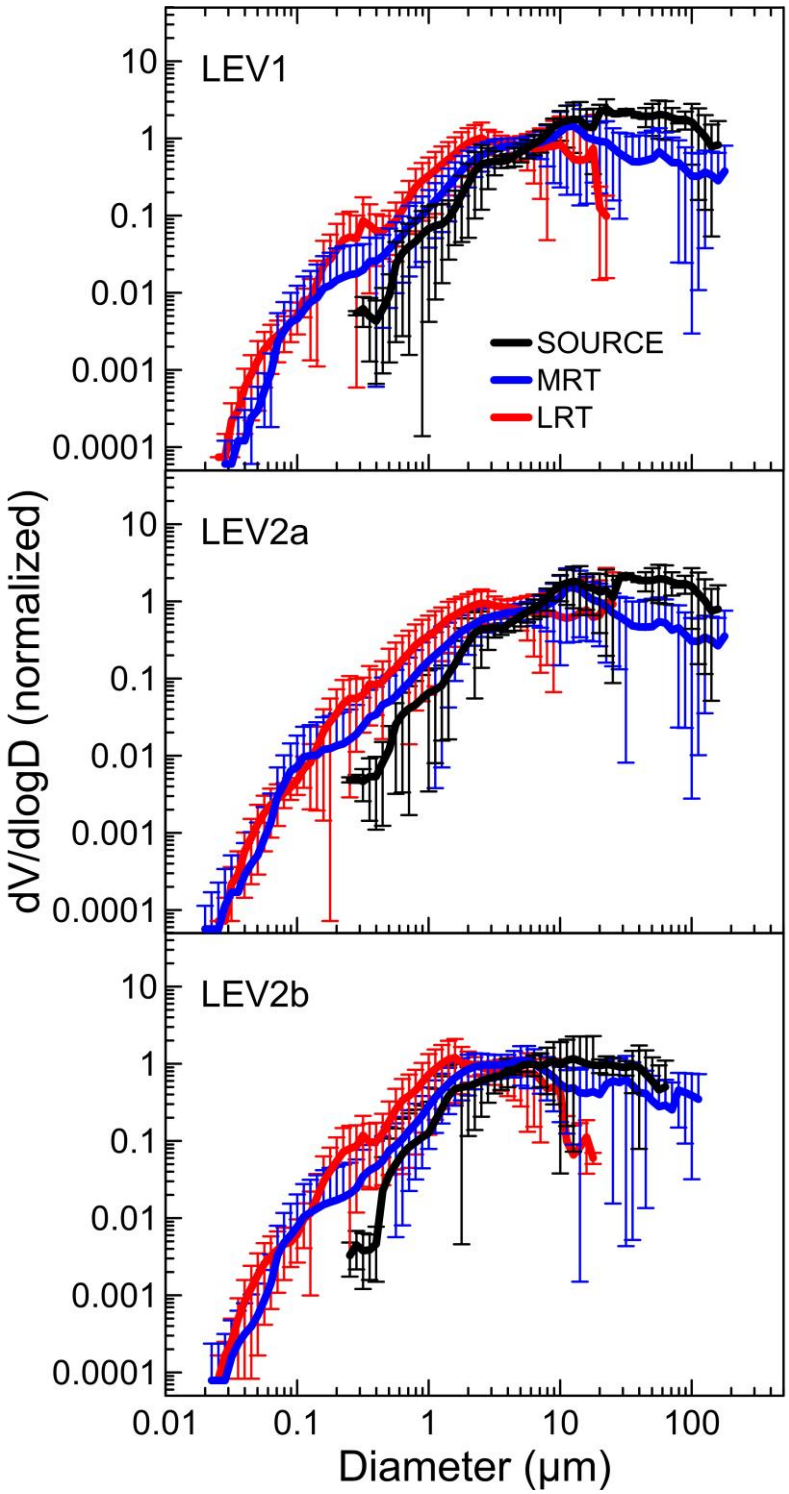

Figure S3. Vertical distribution of the different datasets used in the present analysis for the SOURCE (black), MRT (blue), and LRT (red).

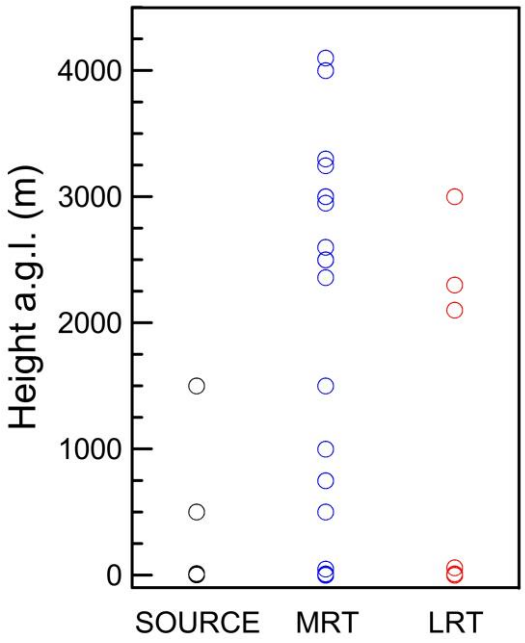

Figure S4. Lognormal size distributions fitting the LEV2a and LEV2b mean values of the three SOURCE; MRT, and LRT dust categories. Parameters (total volume concentration, V_{tot} ($nm^3\ cm^{-3}$), volume median diameter, VMD (µm), geometric standard deviation, σ) for the log-normal modes are indicated in the figure.

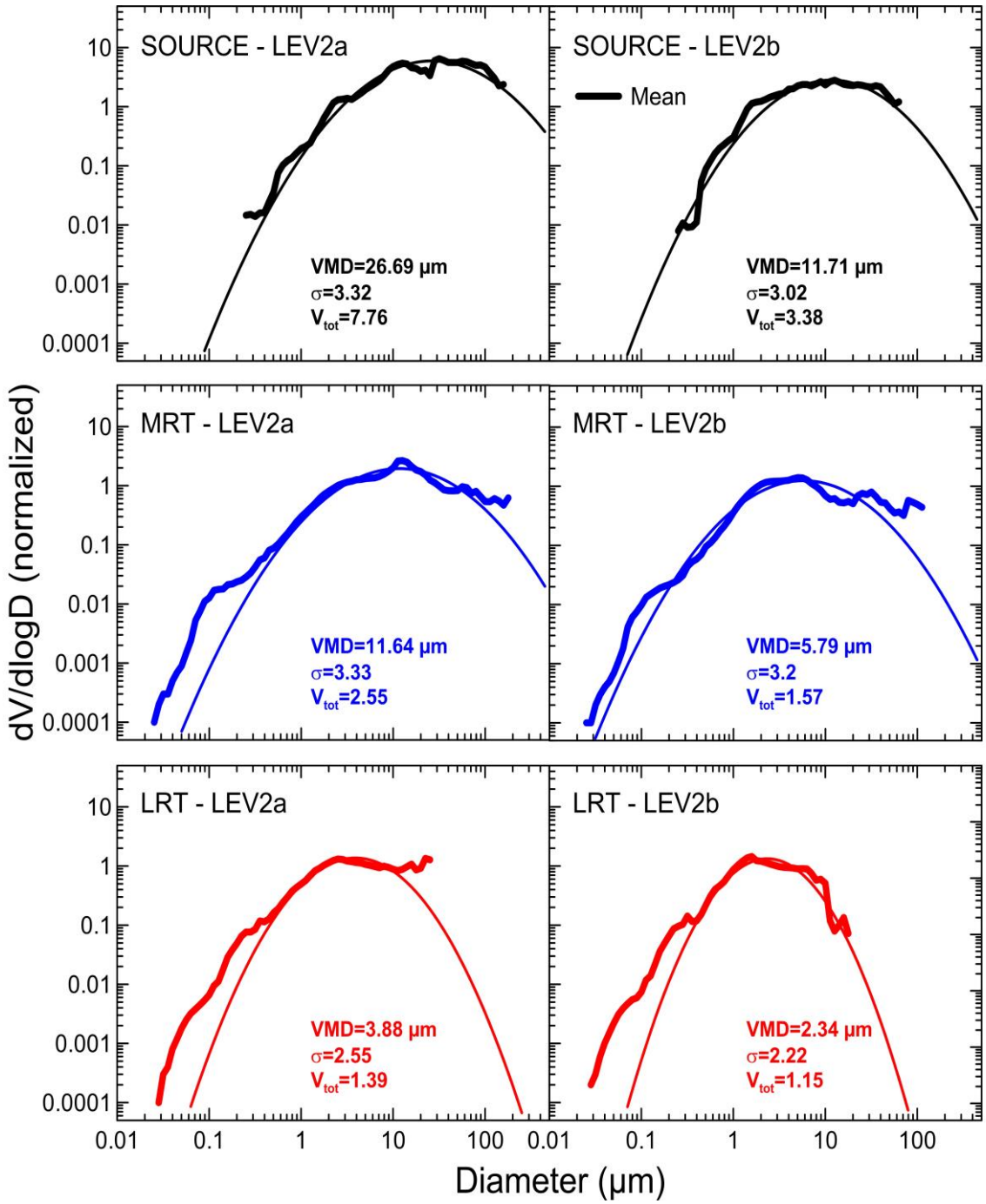

Text S1. Acronyms and year of field campaigns

ACE2= second Aerosol Characterization Experiment (1997)

ACE−ASIA = Asian Aerosol Characterization Experiment (2001)

ADRIMED = Aerosol Direct Radiative Impact on the regional climate in the MEDiterranean region (2013)

AER–D = AERosol Properties – Dust (2015)

AMMA = African Monsoon Multidisciplinary Analysis (2006)

ATTO = Amazon Tall Tower Observatory (2011 −)

BACEX = Barbados Aerosol Cloud Experiment (2010)

CLAIRE−98= Cooperative LBA Airborne Regional Experiment (1998)

DABEX = Dust And Biomass–burning Experiment (2006)

DARPO = Desert AeRosol over Portugal (2006)

DIAPASON = Desert−dust Impact on Air quality through model−Predictions and Advanced Sensors ObservatioNs (2013)

DODO = Dust Outflow and Deposition to the Oceans (DODO1, February 2006; DODO2, August 2006)

Dust−Attack = DUST Aging and Transport from Africa to the Caribbean (2012)

FENNEC = The Saharan Climate System (2010−2012)

FRAGMENT = FRontiers in dust minerAloGical coMposition and its Effects upoN climate (2019)

GAMARF = Ground−based and Airborne Measurements of the Aerosol Radiative Forcing (2008)

GERBILS = Geostationary Earth Radiation Budget Intercomparisons of Longwave and Short−wave radiation (2007)

GoAmazon = Green Ocean Amazon Experiment (2014−2015)

INDOEX= Indian Ocean Experiment (1999)

JADE = Japanese Australian Dust Experiment (2006)

NAMMA = NASA African Monsoon Multidisciplinary Analysis (2006)

PRIDE= Puerto Rico Dust Experiment (2003)

RHaMBLe = Reactive Halogens in the Marine Boundary Layer (2007)

SALTRACE = Saharan Aerosol Long–range Transport and Aerosol–Cloud–Interaction Experiment (2016)

SAMUM = Saharan Mineral Dust Experiment (SAMUM1, 2006; SAMUM2, 2008)

TRACE−P= Transport and Chemical Evolution over the Pacific (2001)

UAE2 = United Arab Emirates Unified Aerosol Experiment (2003)

WIND-O-V's= WIND erOsion in presence of sparse Vegetation (2017)

Text S2. Size instrumentation generalities and acronyms

Documenting the dust size distribution is an experimental challenge. There is no unique in situ instrument covering the natural dynamical range of the mineral dust size and concentration, which can only be represented by a combination of instruments based on different intrinsic particle properties such as density, electrical charge, shape and composition (e.g., Reid et al., 2003a; Formenti et al., 2011; Wendisch and Brenguier, 2013; Mahowald et al., 2014). Light scattering techniques used by optical particle counters (OPC) provide with sizing between approximately 300 nm to 100 µm as optical equivalent diameter referring to a sphere of given refractive index, which scatters the same amount of radiation into a given solid angle as the dust particles would do (e.g., Reid et al., 2003b; Osborne et al., 2008; Formenti et al., 2011; Ryder et al., 2013a; Weinzierl et al., 2017). Microscopy sizing methods, also providing with a large size range, are based on particle collection by filtration or impaction followed by individual particle characterization by transmission (TEM) and/or scanning electron microscopy (SEM) techniques (e.g., Reid et al., 2003b; Kandler et al., 2007; 2009; Chou et al., 2007; McConnell et al., 2008; Ryder et al., 2018). Microscopy provides information on the geometry of projected area particles. Optical array probes (OAP) can be used to measure in situ the geometry of particles and providing two−dimensional projections of them (Ryder et al., 2013; 2018). Techniques based on the Coulter principle can be also used to size insoluble particles suspended in a conductive liquid, providing the geometrical (volume−equivalent) diameter (e.g., Kobayashi et al., 2007). The submicron fraction can be sized in terms of the electrical mobility diameter of a charged particle moving in a static electric field, as done by the Differential or Scanning Mobility Particle Sizer (DMPS, SMPS) (e.g., Muller et al., 2010; Denjean et al., 2016a, 2016b). Aerodynamic particle sizers (APS), measuring the diameter of a sphere of unit density having the same terminal velocity in an accelerated airflow as the irregularly shaped dust particles e.g., (Maring et al., 2003; Reid et al., 2008; Chen et al., 2011). The mass size distribution is measured by multi−stage filtration or impaction sampling coupled with gravimetric or chemical analysis (e.g., Formenti et al., 2001; Reid et al., 2003b).

When retrieving the size distribution of dust over the largest possible diameter range different kind of difficulties arise:

1/ the first one is related to the fact of combining instruments measuring different diameters and the combination is far from being without ambiguity and subject to analysis evaluations and choices;

2/ the second one is related to the size−dependent sampling biases that can affect the measurements, both in the fine and the coarse fractions, and in particular due to the mass inertia of larger particles which are lost in bends and long tubes at the entrance of the instruments (Wendisch and Brenguier, 2013). Largest biases are expected in airborne data from research aircraft due to the lowered sampling efficiencies at low pressure and high aircraft speed (Wendisch and Brenguier, 2013; Sanchez−Marroquin et al., 2019).

In the following we summarize the techniques and spell the acronyms of the different instruments considered in the literature, classified by classes of instruments providing different definitions of the measured diameter. For OPC; the most used instruments for dust size measurements, details on the nominal diameter range and operating wavelength for each instrument type are reported.

Geometrical diameter (volume−equivalent)

- Coulter counter

Projected−area diameter

- Microscopy
  - SEM= Scanning Electron Microscopy
  - TEM = Transmission Electron Microscopy
- OAP = Optical Array Probe
  - CIP = Cloud Imaging Probe

Aerodynamic diameter

- APS = Aerodynamic Particle Sizer
- Multi−stage filtration and chemical analyses

Mobility diameter

- DMPS=Differential Mobility Particle Sizer
- SMPS= Scanning Mobility Particle Sizer

Optical diameter

- OPC= Optical Particle Counter
- CAS = Cloud and Aerosol Spectrometer, nominal diameter range 0.6−50 µm, operating wavelength 680 nm
- CDP = Cloud Droplet Probe, nominal diameter range 0.3 to 50 µm, operating wavelength 658 nm
- CLIMET CI−3100= nominal diameter range 0.26−7.0 µm, operating wavelength not found
- FIDAS 200S= nominal diameter range 0.2−19.1 µm, polychromatic un−polarized LED light source
- FSSP−100= Forward Scattering Spectrometer Probe, nominal diameter range 0.5−47 µm, operating wavelength 632.8 nm
- FSSP−300= Forward Scattering Spectrometer Probe, nominal diameter range 0.275−20.5 µm, operating wavelength 632.8 nm
- GRIMM 1.108= nominal diameter range 0.3−20 µm, operating wavelength 780 nm
- GRIMM 1.109/1.129= nominal diameter range 0.25−32 µm, operating wavelength 655 nm
- LAS−X = nominal diameter range 0.12−7.5 µm, operating wavelength 630 nm
- LOAC= Light Optical Aerosol Counter, nominal diameter range 0.2−100 µm, operating wavelength 650 nm
- Opc MetOne = nominal diameter range 0.49−10.0 µm, operating wavelength 589 nm
- OPC YGK Corp. = nominal diameter range 0.3−7.0 µm, operating wavelength 780 nm
- OPS (model 3330 Optical Particle Sizer, nominal diameter range 0.3−10 µm, operating wavelength
- PCASP = Passive Cavity Aerosol Spectrometer Probe, nominal diameter range 0.1−3 µm, operating wavelength 632.8 nm
- SID = Small Ice Detector, nominal diameter range 2−60 µm, operating wavelength 532 nm
- USHAS= Ultra High Sensitivity Aerosol Spectrometer, nominal diameter range 0.04−1.0 µm, operating wavelength 1054 nm
- WELAS = nominal diameter range 0.3−10 µm, white light source

Text S3. Conversion formulas between diameter definitions

For each diameter type definition this section discusses the treatment applied to convert data into a common geometrical (volume–equivalent) diameter definition both under the assumption of spherical and aspherical particles, as then used to convert data into LEV2a and LEV2b as discussed in the main text and following details in Text S4. The treatment discussed here follows the theory and the treatment proposed and discussed in the literature (e.g., Hinds, 1999, De Carlo et al., 2004 ; Mahowald et al., 2014; Huang et al., 2020, 2021; Formenti et al., 2021).

1/ *geometrical diameter* (or *volume–equivalent diameter*), D_{geo}, is defined as the diameter of a sphere having the same volume as the irregularly–shaped particle. The geometrical diameter is the parameter usually applied in climate models to refer to aerosol particles and it is the target reference diameter in this work. As discussed in Text S2 it can be measured by coulter counters.

2/ *projected–area diameter*, D_{area}, is the diameter of a circle having the same area as the dust particle projected in a two–dimensional image. It is obtained mostly from optical and electron microscopy, which is a diffused technique to size aerosol particles in atmospheric sciences (e.g., Gillette et al., 1972 ; Reid et al., 2003 ; Chou et al., 2008). The microscopy techniques has the advantage of providing image of the particle and to estimate its size directly from the particle visualization, but that shows multiple disadvantages, such as i/ to characterize only two particle's dimensions, therefore requiring assumptions on the third one, ii/ to be highly time consuming and iii/ to have low spatio–temporal resolution since a minimum integration time is required to collect particles on filters to observe in microscopy. For spherical particles D_{area} is equal to D_{geom}. For aspherical dust the D_{area} diameter should be corrected to take into account deviation from sphericity. Following Huang et al. (2021) the relation between projected–area and geometrical diameter can be written as:

$$D_{area} = D_{geom} \frac{\sqrt[6]{AR}}{\sqrt[3]{HWR}} \qquad \text{Eq. S1}$$

where the aspect ratio (AR) and height–to–width–ratio (HWR) are the two parameters used to quantify particle asphericity for dust approximated as tri–axial ellipsoids. Huang et al. (2020) compiled global AR and HWR and found that both parameters deviate from unity and seem to be size independent and being lognormally distributed. They determine a median globally averaged value of 1.7 ± 0.03 for AR and 0.40 ± 0.07 for HWR. For aspherical dust, based on the application of Eq. (S1) and applying a Monte Carlo simulation taking into account the global distribution of AR and HWR, Huang et al. (2021) derived a global average conversion factor of 1.56 to convert D_{area} into a D_{geom} (D_{geom}= D_{area} /1.56).

3/ *aerodynamic diameter*, D_{aerod}, is the diameter of a spherical particle with density of 1 g cm^{-3} having the same aerodynamic resistance as the investigated aerosol. This diameter is measured by an instrument called aerodynamic particle sizer (APS). Also the cascade impactors measure integrated mass as a function of aerodynamic diameter since D_{aerod} is used to classify impactor stages cut off diameters. In the continuum regime (i.e. when a gas can be thought to be as a continuous fluid in flow around the particle, represented by the Knudsen number Kn << 1) the aerodynamic diameter can be converted into a geometrical diameter by the knowledge of the particle density and the dynamic shape factor χ in order to account for the dynamic conditions of sampled particles (De Carlo et al. 2004). The dynamic shape factor is the ratio of the aerodynamic resistance exerted on an aspherical particle to the resistance that would be exerted on a spherical particle with equal volume than the particle under consideration (Hinds, 1999). The relation linking the aerodynamic and the geometric diameter can be written as:

$$D_{aerod} = D_{geom} \sqrt{\frac{\rho_{dust}}{\chi \rho_0}} \qquad \text{Eq. S2}$$

where ρ_{dust} is the density of dust aerosols (assumed to be 2.5 g cm^{-3}, chosen at the mean of the range of desert dust densities as reported in the literature, i.e. 2.1–2.75 g cm^{-3} (i.e. Maring et al., 2000; Reid et al., 2003a; Fratini et al., 2007) and ρ_0 is the standard density (1.0 g cm^{-3}). For spherical dust, the application of Eq. (S2) to a shape factor of 1 result in a conversion factor of 1.58 to correct the D_{aerod} into a D_{geom} (D_{geom}= D_{aerod} /1.58). For aspherical dust approximated as tri−axial ellipsoids, Huang et al. (2021) applied the global AR and HWR compiled in Huang et al. (2020) to calculate the dynamic shape factor for dust aerosols and used these factors to determine a size−invariant conversion factor of 1.45 that allows to transform the aerodynamic into the geometric diameter based on Eq. (S2) (D_{geom}= D_{aerod} /1.45).

4/ *electrical modibility diameter*, D_{mob}, the diameter of a sphere with the same migration velocity in a constant electric field as the particle of interest. This diameter is what is measured by the DMPS or SMPS and can be converted into a geometrical diameter based on the knowledge of the dynamical shape factor χ as:

$$D_{geom} = \frac{D_m}{\chi} \qquad \text{Eq. S3}$$

For spherical dust, a shape factor of 1 result in an equality between D_{mob} and D_{geom}. For aspherical dust approximated as tri−axial ellipsoids, a global mean shape factor of 1.19 is estimated starting from the 1.45 D_{aerod} to D_{geom} ratio by Huang et al. (2021) and inverting Eq. S2.

5/ *optical diameter*, D_{opt}, the diameter of an aerosol showing the same intensity of scattered light than the dust aerosols. The optical diameter is usually measured by means of optical particle counters (OPCs), recording the scattered−light intensity over a specific angle range and associating a particle size based on the knowledge or assumption of the index of refraction of the particle under investigation. Complex refractive index assumptions and the use of optical theories adapted to aerosol shape are used to associate a scattering intensity to a particle size, therefore allowing to convert the optical diameter into a geometrical diameter. In this study we take advantage of the database developed by Formenti et al. (2021) who evaluated size−dependent correction factors for dust under both the assumption of sphericity and non sphericity and for varying refractive index for various OPC models (CDP−300, FSSP−300, GRIMM1.129/1.109, and PCASP−100). The corrections factor by Formenti et al. (2021) for spherical dust and assuming a refractive index of 1.53−0.003i in the visible (value that is at the average of the dust global values reported in Di Biagio et al. 2019 in the range 370-950 nm, therefore covering the range of operation OPC wavelengths as details in Text S2) are applied to correct the different datasets. For the GRIMM 1.108 OPC model, for which the conversion was not provided in Formenti et al. (2021), the conversion in Formenti et al. (2011) for the refractive index of 1.53−0.002i calculated under spherical assumption is considered. In order to be applied in the present study the D_{opt} to D_{geom} conversion factors are recalculated at the interpolation diameters used for LEV1 to LEV2b data. For OPCs models as listed in Text S2 and not treated in the Formenti et al. (2011) and (2021) work, the correction corresponding to the most similar OPC model (operating wavelength, sensing angles) within those in Formenti et al. (2011) or (2021) is used. Specific assumptions are detailed in Text S4 for each dataset involved in the specific case.

To take into account for aspherical effects in OPCs corrections, the D_{opt} to D_{geom} spherical and aspherical calculations in Formenti et al. (2021) and Huang et al. (2021) are used. These studies report for different OPCs the optical to geometrical diameter conversion factors both in the assumption of spherical homogeneous particles $(D_{geom})_{spherical}$ and tri−ellipsoids dust $(D_{geom})_{aspherical}$. For the calculations the refractive index of 1.53−0.0032i is used in Formenti et al. (2021) for CDP, FSSP, GRIMM and PCASP OPCS considered here, whereas the refractive index values of 1.48−0.0012i and 1.51−0.0038i are used in Huang et al. (2021) for the CLIMET and the WELAS, respectively. The size−dependent aspherical to spherical ratio ($ASR(D_{geom})$) correction function, $ASR(D_{geom})=(D_{geom})_{aspherical}/(D_{geom})_{spherical}$, obtained by averaging the ASR function obtained for the different OPC models is shown in Figure S1. The ASR function represent the change in optical to geometrical correction when aspherical dust is assumed in

spite of spherical dust. The average ASR(D_{geom}) function is taken constant at the value of 1 below 0.2 µm, when no single OPC data are available for the ASR evaluation, and at the value of 0.39 above 30 µm diameter. The 0.39 value is the average obtained for between 20 and 30 µm diameter when at least three OPCs ASR datasets are available for averaging. The ASR(D_{geom}) function is then used to include the effect of asphericity in OPCs data correction, as discussed in Text S4.

In this study we decided to define a common ASR(D_{geom}) function for all OPCs instead of defining a different one for different instrument models. This is due for two main reasons: 1/ not all OPC models used from in situ studies have specific ASR(D_{geom}) documented from Formenti et al., (2021), Huang et al. (2021) or their study; 2/ several datasets considered here combine several OPCs to get their final reported size distribution and unknown information are given on how this merging is done, therefore it is unknown how to combine different ASR(D_{geom}) correction functions in these cases. Given the spread in the ASR(D_{geom}) functions for the different models, it is clear that the approach of using a common average ASR is over simplistic. However, and also given the heterogeneity of the dataset ensemble, this treatment allows to provide a global evaluation of for asphericity effects in the dataset ensemble.

Text S4. In situ dataset description

The following text describe the in situ datasets included in the present study and ordered chronologically, providing brief schematic context about the field campaigns and experiments that lead to size data measurements and the relevant technical details about instrumentation and data analysis in the original papers. This dataset description is complementary to other size dataset descriptions already provided in other studies and considering part of the same datasets used here (i.e., Kok et al., 2017; Adebiyi et al., 2020). Specific assumptions for the data treatment are also provided for the datasets concerned in order to complete the data analysis description in Texts S3 and in the main manuscript in Sect. 2.2 and 2.3 . Each dataset start with a three−field indication of the techniques used to measure size (microscopy, OPC, DMPS, DMPS+APS, ….), the indication of where the data have been acquired (ground−based or airborne), and the diameter definition as provided in the original publications. These information (reported in blue character here) are schematically synthetized in Table S1. For each dataset we also indicate clearly how the data are retrieved (contact with author, data from repository, digitalization, ..) and in which format they are expressed in the original paper. For datasets relying on multiples instruments and for which a choice on the main "dominant" instrument is done for converting to LEV2a and/or LEV2b data (see discussion in Sect. 2.2, 2.3, 2.4 in the main manuscript) we also add specification in the text of which is the main instrument considered in our analysis for data corrections. Error bars for each dataset are either the values provided in the original dataset or the variability of averaged data, when reported. When not reported, but possible, we calculate the average and standard deviation of multiple datasets. Otherwise, error bars are not reported.

It is worth to mention that further observations of size distribution for dust at source have been also found in the literature but not considered in the present analysis, including the work by (Kandler et al., 2009) during the SAMUM−1 campaign, and the observations by Schutz and Janicke (1974), Schutz (1981), D'Almeida (1987), Gillette and Nagamoto (1993), and Sviridenkov et al. (1993) in the Sahara, the Sahel, and Tadjikistan. These data are not considered in the main analysis mainly because of the lack of detailed information on the techniques or data acquisition and treatment, preventing from a clear assessment of their quality and/or classification, whereas for the Kandler et al. (2009) dataset acquired close to source regions in Morocco, the dataset was reported to be contaminated by very large saltation and sand−blasting grains from the soil.

The datasets considered in the present study are listed in the following.

- (Gillette et al., 1972, 1974) and Gillette (1974): microscopy, ground−based, projected−area diameter. These authors reported first field measurements of the size−resolved vertical dust flux based on measurements they performed on one sandy loam, two fine sand, and two loamy fine sand soils. Observations were in Texas and Nebraska and included a range of wind speeds. Measurements were performed using a two single−stage impactors installed at heights of 1.5 and 6 m above the ground level. The aerosols collected on filters were analyzed by optical microscopy technique to retrieve the size−resolved vertical dust flux between 1 and 20 µm diameter range. Data from Gillette studies were treated and synthetized in Kok et al. (2017) and we assume the same dataset as Kok et al. in the present analysis. Original data are expressed as size−resolved aerosol fluxes (dN cm^{-2} s^{-1}) In this study we take the dV/dlogD data normalized at the integral of 1 between 0.2 and 20 µm as published in Kok et al. (2017). Data are obtained from J. Kok (personal communication).
- (Schütz et al., 1981): microscopy, ship−based, projected−area diameter. They reported size distribution data for dust close to the source, labelled as Sahara and corresponding to SAL observations, and data for transport distances of 1000, 2000, and 5000 km obtained from surface−level measurements from the German vessel Meteor while crossing the Atlantic Ocean at a latitude of about 15°N. In this study we used size distribution data for transport of 1000 km as representative of the MRT conditions, and data for 5000 km as representative of LRT. Geographical coordinates were defined arbitrarily based on information from the paper and transport distances.

Original data are reported as dV/dlogR. Data are digitalized from the original publication in their Figure 14.5).

- **(d'Almeida, 1987):** microscopy, ground–based, projected–area diameter. Aerosol particles were collected on filter substrate, then dissolved in an organic liquid to put them in suspensions, and further counted with scanning electron microscopy (d'Almeida and Schütz, 1983). The procedure avoided charging effects on the sample surface and data were corrected to account for the filter collection efficiency. Measurements were taken at three sites in Senegal, Mali and Niger between February–March 1979, and January–February 1982. Observations corresponding to sandstorm and wind carrying dust conditions are shown in their Figure 3. The wind carrying dust represents dust after 1 or 2 days after the heavy sandstorm episode. In the present study we use the wind carrying sust observations as representative of MRT conditions, whereas the sandstorm dataset was not considered because of lacking information on the age of the plume to properly identify the data as SOURCE category. Original data are reported as dN/dlogD. Data are digitalized from the original publication in their Figure 3.
- **(de Reus et al., 2000):** DMPS + OPC (PCASP, FSSP–300), airborne, geometrical diameter. Airborne observations of the aerosol size distribution were retrieved during the Second Aerosol Characterization Experiment (ACE 2) near Tenerife, Canary Islands, in July 1997. The size distribution of dust aerosols was measured in the submicron range by combining a DMA and a CPC from 0.02 up to 0.15 µm and an OPC PCASP to get aerosol size between 0.11 and 3.5 µm. The PCASP was calibrated with ammonium sulphate aerosols below 1 µm diameter and with PSL above 1 µm. An FSSP–300 was installed on the fuselage and measured up to 31 µm diameter. It is reported that the FSSP is calibrated with a refractive index of 1.55–0.004i for Saharan dust aerosols. Measurements correspond to the dust aerosols measured at 4 km altitude. In our treatment we assume the OPC to be the main instrument of reference for LEV2b corrections. Original data are reported as both dN/dlogD, dS/dlogD, and dV/dlogD in their figure 4. We considered the dV/dlogD ($\mu m^3\ cm^{-3}$) from Figure 4c. Data are digitalized from the original publication.
- **(Maring et al., 2000):** SMPS+APS, ground–based, geometrical diameter. In their work they reported dust size distribution measurements in the free troposphere at 2360 m at Izana, Tenerife (Canary Island) in July 1995. The size distribution was derived by combining a TSI Scanning Mobility Particle Sizer (SMPS) Model 3934L sizing aerosols from 0.013 to 0.85 µm with a TSI Aerodynamic Particle Sizer (APS) Model 3310 measuring in the range going from 0.8 up to >15 µm aerodynamic diameter. Aerosols with diameters >0.6 µm measured at Izana in July 1995 appeared to be almost exclusively mineral dust. Dust mass closure calculations in their study indicated that the dry dust aerosol density is 2.0 $g\ cm^{-3}$, and this value was used in the original publication to convert aerodynamic to geometric diameters. In absence of further information we assume the shape factor of dust to be equal to 1 in the original data analysis. In our treatment we assume the APS to be the main instrument of reference for LEV2a and LEV2b corrections. We report here the synthesis of their data as dV/dlogD peak–height normalized distribution as reported in Maring et al. (2003) in their Figure 3. Data are digitalized from the original publication.
- **(Formenti et al., 2001):** cascade impactor, ground–based, aerodynamic diameter. Measurements were acquired in Brasil at the site of Balbina during the CLAIRE–98 experiment. Mass size distribution was derived from elemental analysis of dust samples collected on a 12 stages small deposit–area low–pressure impactor (SDI) operated at 11 $L\ min^{-1}$. The authors indicated that at this flow rate, the cut points were 8.5, 4.1, 2.7, 1.7, 1.1, 0.77, 0.59, 0.34, 0.23, 0.15, 0.086 and 0.045 µm as equivalent aerodynamic diameters. At Balbina, transport of mineral dust from Africa within the NE trade winds took place without interruption from 24 to 27 March 1998, for dust originated across the Moroccan coast for trajectories arriving below 800 hPa on the 25th March. The mass size distributions dM/dlogD of several elements (Al, P, S, Cl, K , Ca, V, andZ n) were reported in their Figure 11 for dust sampling on the 25 March. The size distribution of the Al element is considered here as

representative of dust. Original data are mass size distribution dM/dlogD as ng m^{-3}. Data were digitalized from the original paper, their Figure 11.

- **(Bates et al., 2002):** DMPS+APS, ground–based, geometrical diameter. Aerosol number size distributions were measured aboard the Research vessel Ronald H. Brown during the Indian Ocean Experiment (INDOEX) 1999 Intensive Field Phase. Measurements combined a differential mobility particle sizer (DMPS) working on 27 size bins with midpoints diameters ranging from 0.022 to 0.9 µm and an aerodynamic particle sizer (APS), covering a size range between 0.6 and 9.6 µm aerodynamic diameter. Taking into account inlet efficiency and instrumental corrections, it resulted that the size was measured from 0.02 to 7 µm geometric diameter at 55% relative humidity. In doing diameter conversions the authors assumed an aerosol density of 1.33 g cm^{-3} as indicated in Quinn et al. (2002). The aerosol number size distributions measured during the campaign in the Indian Ocean marine boundary layer were categorized into eight air mass source regions based on air mass back trajectories. We report here the average size distribution from their Figure 4 corresponding to the average for the SHmX Southern Hemisphere marine Extratropical air mass condition, corresponding to a transport time of up to 108 h that we associate to MRT category, and also the retrieved mineral dust data from their Figure 5 as measured during the AEROSOL99 campaign and corresponding to a dust transport of 43h. In our treatment we assume the APS to be the main instrument of reference for LEV2a and LEV2b corrections in both datasets. In absence of further information we assume the shape factor of dust to be equal to 1 in the original data analysis. Data are reported as both dN/dlogD and dV/dlogD and we took the volume data as reported in their Figures 4c and 5b. Data are digitalized from the original publication.
- **(Maring et al., 2003):** SMPS+APS, ground–based, geometrical diameter. They reported measurements of the dust size distribution measured at the sea level in Puerto Rico during PRIDE in July 2000. Size distribution measurements and setup were similar to those of Maring et al. (2000) at Izana, with the only difference that the sample inlet in Puerto Rico, which is a humid environment with often RH>80%, was heated so to reduce RH to values below 50%. Measurements during PRIDE confirmed, as observed at Izana in Maring et al. (2000), that aerosols with diameters >0.6 µm consisted of dust and sea salt, in contrast with the accumulation mode particles. A dust–dominated size distribution for PRIDE was obtained by subtracting to the campaign average the size distribution measured for periods of high sea salt concentrations based on concurrent chemical analyses. A dust mass closure calculation indicated a dry dust aerosol density of 2.0 g cm^{-3}. This density was used to convert all aerodynamic to geometrical diameters. In our treatment we assume the APS to be the main instrument of reference for LEV2a and LEV2b corrections in both datasets. We report here the synthesis of the data reported from these authors as dV/dlogD peak–height normalized distribution as in their figure 3. Data are digitalized from the original publication.
- **(Reid et al., 2003a):** microscopy, airborne, projected–area diameter. Atmospheric dust samples were collected by Piper Nvajo aircraft at various elevations in the SAL during the PRIDE field campaign in Puerto Rico in June–July 2000. The samples for single particle analysis were collected at a flow rate of 5 L min^{-1} by means of a nearly isokinetic inlet with a 50% cutoff at 10 µm for dry dust. The authors noted in the paper that anyhow some large particles up to 20 µm in diameter could be collected, particularly at low humidity conditions. The size distribution of dust aerosols was obtained by the analysis of SEM microscopy images. Particle area and volume distributions are presented in their Figure 8 for selected dust samples. Estimated volume distributions are modelled to be lognormal, with volume median diameters (VMD) from 7 to 9 µm, and geometrical standard deviations on the order of 1.6 to 1.8. Original data are reported as area and volume normalized distribution in their Figure 8. We consider the volume size distribution in our study and we calculated the average and standard deviation of the data reported in Figure 8 for dust in the SAL (4 datasets between the 16th and the 22 July). Data are digitalized from the original publication.
- **(Reid et al., 2003b):** 2 datasets: (cascade impactor, ground–based, geometrical diameter) && (OPC, airborne, optical diameter). In their paper Reid et al. report a summary of size observations as

obtained during the PRIDE campaign in 2000 at Puerto Rico. Some of the data discussed in this paper were summarized elsewhere, in particular the ground based APS observations at Puerto Rico were reported in Maring et al. (2003) and the complete analysis of the airborne microscopy samples was reported by Reid et al. (2003a) and discussed just above. In this paper their reported additional data of dust size distributions recorded at Puerto Rico in July 2000 as obtained by means of cascade impactor observations at the Cabras Island site and airborne OPC data. The cascade impactor used during PRIDE was the University of Miami MOUDI system (MicroOrifice, Uniform–Deposit Impactor) collecting samples in 8 stages with 50% cut points at 22, 12, 7.6, 3.8, 2.2, 1.24, 0.71, and 0.41 µm. One integrated 68 hour sample obtained in the period 21 to 24 July was used to determine Al, Br, Cl, Mn, Na, V, I, and K elements (neutron activation analysis, NAA). The dust mass size distribution was derived by considering as tracer the Al, and so the Al mass distribution was taken as representative of dust aerosols. The conversion between Al and dust mass was 12.5 or 8% of mass. Aerodynamic to geometrical conversion was performed assuming a conversion factor of 1.4 as the square root of the dynamic shape factor divided by particle density. Both the aerodynamic and the retrieved geometrical distributions are presented in Figure 6 of Reid et al. for the dust event of the 21–24 July 2000. To note that a second cascade impactor, the Devis Rotating Drum (DRUM), was also used in Puerto Rico to derive the dust mass distribution by XRF analysis. However, since mass distribution data are only reported as a function of the aerodynamic diameter in that second case, and because the upper channel was at only 5 µm diameter, we do not consider this further dataset in our analysis. Additional observations of the dust size distribution were reported by Reid et al. considering the airborne measurements of two OPCs (an FSSP–100 and a PCASP–100X) wing–mounted on the Navajo aircraft. The PCASP provided the dry particle size distribution (RH =35–40%), whereas the FSSP–100 inferred the ambient size distribution. Both instruments were calibrated before and after the campaign with PSL particles. The number, surface and volume size distribution for five dust events in July 2000 for the OPCs are reported in their Figure 10. In the present study we consider the average and standard deviation of these observations. In our treatment we assume the FSSP–100 to be the main instrument of reference for LEV2a and LEV2b corrections for OPCs data. For LEV2a data correction we assume that the optical to geometrical conversion is the same that the one estimated for the FSSP–300 as reported in Formenti et al. (2021), despite a smaller opening receiving angle (5–13°) in the FSSP–100 model than in the FSSP–300 model (3–15°). Original data are reported as mass size distributions from the cascade impactors and as number, surface and volume size distribution for the OPCs. Data are digitalized from the original paper from their Figure 6 for cascade impactor data and from their Figure 10 for OPCs data.

- (Clarke et al., 2004): OPC, airborne, optical diameter. These authors report measurements taken during the ACE–Asia and TRACE–P campaigns in the Sea of Japan (between Koran and Japan) in the spring (24 February to 10 April) of 2001. Size distribution between diameters of 0.1 and 10 µm was measured by means of an optical particle counter (OPC, a modified LAS–X, Particle Measurement Systems, Boulder, Colorado) operated at 150°C and then at 300°C to remove volatile species. OPC was calibrated with a refractive index of 1.588 up to 2 µm and 1.54 above that size, however dust absorption or asphericity were not accounted for and data are reported as optical diameter. A synthesis of dust size distribution defined a "reference dust" was calculated between surface and 6 km height merging observations. The contribution of black carbon was subtracted from the ensemble of field sizes. The time of transport is not defined in the paper and we classified this dataset as MRT. In our treatment, and specifically for LEV2a data treatment, we assume that the optical to geometrical conversion is the same that the one estimated for the PCASP–100 as reported in Formenti et al. (2021). As a matter of fact the physical properties of the LAS–X (operating wavelength of 630 nm and opening angle of 35 to 120°) are very similar to the PCASP one. We report the size for the reference dust case as dN/dlogD as in their Figure 5c. Data are digitalized from the original publication.

- **(Fratini et al., 2007):** OPC, ground–based, geometrical diameter. These authors used eddy covariance to measure the size–resolved flux of dust emitted over a sandy soil in the Gobi desert in Inner Mongolia, China. They measured the dust particle concentration by means an optical particle counter (OPC, CLIMET CI 3100), which sized particles within an equivalent aerodynamic diameter range of 0.35–9.5 µm. The optical diameter was converted into an aerodynamic diameter following the formula $D_{aerod} = D_{opt} (\rho_{dust})^{0.5} \cdot f(D_{opt}, m)$, where the $f(D_{opt}, m)$ function was estimated to be around 0.85 as calculated assuming a refractive index of 1.53–0i and a soil particles density of 2.5 g cm^{-3}. It resulted that the $D_{aerod}=1.35 \cdot D_{opt}$. These measurements converted in aerodynamic diameter were then further corrected to geometric diameter by applying Equation (2) assuming a dust density of 2.5 ± 0.2 g cm^{-3} and a dynamic shape factor of 1.4 ± 0.1 in (Kok et al., 2017). In this study we take data as reported in Kok et al. (2017) work and corresponding to the average of the three datasets shown in their Figure 10. Note that the Fratini et al. data > ~ 5 µm in diameter are unreliable because of the cutoff of the inlet system (Fratini personal communication as reported in Kok et al., 2017). In our treatment, and specifically for LEV2b conversion, we treat the Fratini dataset as aerodynamic diameter data following the approach from the original paper and the Kok et al. further analysis. Original data are fluxes as dN cm^{-2} s^{-1} or µg cm^{-2} s^{-1}. We took the treated data from Kok et al. (2017) as the average and standard deviation of the three cases in their Figure 10. Data were obtained from J. Kok (personal communication).
- **(Kobayashi et al., 2007):** Coulter multisizer, ground–based, geometrical diameter. Aerosol sampling was conducted at four sites in Japan at Nagasaki (32°45N, 129°52E), Okayama (34°39N, 133°54E), Kofu (35°39N, 138°34E), and Tokyo (35°41N, 139°45E) in the period spring 2003 to spring 2004 and size distribution was measured with a Coulter multisizer providing the number concentration of water–insoluble aerosol particles in the diameter range of 0.4–12 µm. Springtime was chosen as the time of the year when the Asian dust phenomena typically occur. The size distributions retrieved for the same Asian dust air mass varied at each sampling site and the volume mode diameter ranged from 1.4 to 2.2 µm, reducing when going from west to east. The volume mode diameter was lower than identifed in other Asian outflows, an observation explained by the possible internal mixing of Asian dust with other components and/or due to the breaking/dispersion of particles aggregates by ultrasonic shaking during extraction. The experimental protocol, improved for sampling in 2004, resulted in a larger dust mode in the range of 1–10 µm. Data for this improved configuration were reported by these authors for two dust events measured at Kofu in March – April 2004. The measured mode diameters obtained by fitting with multi lognormal functions the data were 2.6–3.1 and 4.3–5.6 µm in these 2 Asian dust events. Data for the Kofu event are considered in the present analysis. The time of transport is not defined in the paper and we classified this dataset as MRT. Original data are expressed as dV/dlnD up to 10 µm from their Figure 7. We consider here the average and standard deviation of data for two separate events (E2 to E4, identified as E1 – episode1, and E5 to E8, identified as E2 – episode2) corresponding to the two identified Asian dust episodes. Data were recalculated from the lognormal parameters shown in the original publication.
- **(Otto et al., 2007):** DMA + OPC (PCASP, FSSP–300), airborne, optical diameter. These authors report on aerosol measurements acquired during the Aerosol Characterisation Experiment (ACE–2) flights on 8th of July 1997 about 50—200 km off the coast of Northern Africa close to Canary Islands. The aerosol size distributions was measured by five instruments, including Condensation Particle Counter (CPC), Differential Mobility Analyser (DMA), and PCASP and FSSP OPCs, and the data treatment followed the one described in (de Reus et al., 2000). During the flight a dust layer extending from 2.7 to 5.8 km altitude was measured. Vertical–resolved size distribution data averaged over 100 m height were reported by the author in their Figure 3. Original data are expressed as dN/dlogD up to 31 µm form their Figure 3, we consider data at three specific levels (2700 m, 4000 m, 5500 m) where the dust layer was identified. Data are digitalized from the original publication.
- **(Chou et al., 2008):** microscopy, airborne, projected–area diameter. Airborne aerosol measurements were performed during the AMMA / DABEX campaign between 13 January and 3 February 2006 on

board of the UK Bae−146 research aircraft. Flights explored the Western Africa and Sahel regions. The aerosol size distribution was retrieved for dust samples collected during 4 flights between 21 and 30 January 2006 and corresponded to straight−levelled runs portions of the flight. The size distribution of dust particles was estimated by combining aerosol counting from the analysis of SEM (17 size classes ranging from 0.25 to 10 µm) and TEM (19 size classes ranging from 0.01 to 7 µm) microscopy images. The retrieved size from microscopy analysis was in good agreement, and particularly below 0.5 µm diameter, with observations obtained from a wing−mounted OPC as reported in (Osborne et al., 2008). For one of the four analyzed samples (B165N7) the authors identified the presence of anthropogenic particles as evidenced in microscopy images. We consider in this study the average and standard deviation of the size distribution for the four dust cases reported by Chou et al. in their Figure 6. Original data are reported as dN/dlogD in their Figure 6 as the combination of TEM (0.05 to 0.5 µm) and SEM (0.5 to 10 µm). Data were obtained from P. Formenti (personal communication).

- (McConnell et al., 2008): OPCs, airborne, optical diameter. Measurements of dust size distribution were performed during the DODO campaign based at Dakar, Senegal, off the coast of North Africa. The DODO project occurred on two phases: a first one between 7 and 16 February 2006 (DODO−1), and the second one between 22 and 28 August 2006 (DODO−2). During the airborne operations a combination of wing−mounted OPCs were used including a PCASP and a cloud droplet probe (CDP−100). Additionally, optical microscopy on bulk filters were used to measure dust size distribution up to diameter of 40 µm. We consider two datasets in this study, separately for the DODO−1 and the DODO−2 observations as obtained from the combination of PCASP and CDP observations. In our treatment, and specifically for LEV2a and LEV2b conversion, we assume that the main OPC data are those from the CDP, therefore optical to geometrical diameter corrections are taken from calculations of Formenti et al. (2021) for this OPC model. Original data are reported as dN/dlogR normalized to the total number concentration as obtained for DODO−1 (retrieved from Figure 8 in Osborne et al. (2008), identified as dataset McConnell−1) and as dV/dlnR normalized at the value at R=1 µm for DODO−2, retrieved from Figure 7 in McConnell et al. (2008) (identified as dataset McConnell−2). Data are digitalized from the cited publications.
- (Osborne et al., 2008): OPC, airborne, optical diameter. Aerosol measurements were performed during the AMMA/DABEX campaign on board of the UK Bae−146 research aircraft using two OPCs: a wing−mounted Passive Cavity Aerosol Spectrometer Probe 100−X (PCASP) measuring in the diameter range 0.1−3.0 µm and a PCASP−X measuring in the range 0.1−10 µm diameter mounted inside the aircraft cabin that uses a virtual impactor inlet to measure particles up to diameter of 10 µm. It is reported in the paper that the size measurement efficiency was 100% in all size diameters for the PCASP wing−mounted, but not for the PCASP−X. In their paper, Osborne et al. [2008] found that the PCASP−X consistently overcounts when compared to the wing PCASP, and this was associated to a problem with the sample flow. In order to extend the size range of measurements from the wing PCASP, these authors corrected the PCASP−X by rescaling it to match the PCASP data in the region of overlap. They analyzed in their paper the impact of refractive index and non−sphericity in the PCASP measurements but reported data as calibrated for PSL particles and spherical assumption. In our treatment for LEV2a and LEV2b conversion, we assume the PCASP optical to geometrical diameter corrections calculated from Formenti et al. (2021) and extrapolated into a larger diameter range in our study to apply to both PCASP and PCASP−X. We report here the mean aerosol size distribution from the DABEX ‘‘pure’’ dust cases from the northeast of Niamey across the accumulation and coarse modes as shown in their Figure 8 and 9 and reported as dN/dlogR normalized to the total number of particles. Data are digitalized from their Figure 9.
- (Rajot et al., 2008): OPC, ground−based, optical diameter. Data from Banizoumbou (Niger) during the AMMA campaign in 2006 ware used to derive statistics of dust size distribution under different conditions. Size data were obtained from optical particle counter (OPC, Grimm 1.108) measurements and were published as not corrected for the refractive index of dust. The OPC was installed behind

an Isokinetic Particle Collector inlet having a passing efficiency of about 50% at 40µm particle diameter. The used OPC measured up to ~30µm, but the authors discuss the possible presence of an additional coarser mode not detected by the used OPC. Data from their Figure 17 for local erosion events, labelled as L in their Figure, and for dust advected from distant sources, labelled ad D in their Figure are considered in the present study as representative of SOURCE and MRT class events. Original data are dM/dlogD normalized by total mass. The average and standard deviation of the ensemble of D and L cases is considered in the present analysis. Data were obtained from J. L. Rajot (personal communication).

- **(Reid et al., 2008):** APS, ground–based, aerodynamic diameter. As part of the United Arab Emirates Unified Aerosol Experiment (UAE2), the size distribution and chemistry of dust particles were measured for the months of August and September 2004 at an Arabian Gulf coastal site impacted by dust from several sources within southwest Asia. A TSI aerodynamic particle sizer model 3321 was used in the campaign. The APS sampled air from a common inlet through a heated (RH < 35%) line. The primary surface site utilized for the study was the Mobile Atmosphere Aerosol and Radiation Characterization Laboratory (MAARCO), located 50 km north of Abu Dhabi, UAE. The site, which was away from city plumes, mostly sampled air masses representative of the Arabian Gulf and the interior desert. Continuous coarse mode size distributions were measured during the campaign. The authors report data divided as Groups A and B in their Figure 2d, which reflect the two extremes in size for dust observations. Group A, with the smallest volume modal diameter (3.3 µm), consisted of daily samples from 13 and 14 August and 23 September. Conversely, for the largest sized particles in group B (11, 12, 15, 30, and 31 August; 1, 12, 15, 16, 25, and 26 September) the 6 µm volume mode was reported to be dominant compared to the 3 µm mode. Original data are reported as dV/dlnD as aerodynamic diameter. Data are digitalized from their Figure 2d.
- **(Sow et al., 2009):** OPC, ground–based, optical diameter. In their study Sow et al. used two optical particle counters (OPC, Grimm 1.108) at heights of 2.1 and 6.5 m to measure the size–resolved vertical flux of dust aerosols larger than 0.3 µm in diameter. They reported measurements acquired during three dust storm events in Niger and corresponding to an average wind friction speed between 0.4 and 0.6 m s^{-1}. Size data obtained from optical particle counter measurements were published as not corrected for the refractive index of dust. Original data are fluxes as dN m^{-2} s^{-1}. In our analysis we consider the average and standard deviation of the three cases shown in their Figure 9. Data are obtained from J. Kok (personal communication).
- **(Wagner et al., 2009):** OPC, airborne, geometrical diameter. In situ measurements of dust size distribution were performed in May 2006 over Portugal as part of the Desert Aerosols over Portugal (DAPRO) project affiliated with the SAMUM experiment. Airborne observations were performed from the FALCON aircraft using the same instrumental configuration and data treatment as in Weinzierl et al. (2009), with an high spectral resolution lidar additionally installed on the aircraft. Measurements of the size distribution between 0.01 and 35 µm diameter obtained at 2300 m and 3245 m height over Évora on 27 May 2006 were presented in their Figure 9. Ground based measurements of the size distribution were additionally obtained at the ground with an APS but we only considered airborne data in the present analysis. Original data are as dN/dlogD at STP conditions as reported in Figure 9 in Wagner et al.. Size distribution data at the two different heights were averaged and used as a single dataset in the following analysis. Data were digitalised from the original paper, their Figure 9.
- **(Weinzierl et al., 2009):** OPC, airborne, geometrical diameter. These authors reported on size distribution observations acquired during the SAMUM1 airborne campaign from the German Center for Aviation and Space Flight DLR Falcon flights over Morocco in May and June 2006. Size distribution measurements were obtained from a set of different OPCs both wing–mounted or inside the aircraft cabin sampling aerosols through an isokinetic inlet with a 50% passing efficiency at about 2.5 µm in diameter at the ground and 1.5 µm at 10 km. Size instrumentation included a wing–mounted FSSP–300 measuring particles with diameters between 0.3 and 30 µm, three Condensation Particle

Counters (CPCs, heated with a thermal denuder at 250°C) and a Grimm OPC. The three CPCs measured non−volatile particles in nucleation, Aitken, and accumulation mode, respectively, while the Grimm OPC measured non−volatile size distribution below 2.5 µm. The visible refractive index used to correct OPC dust data was 1.551−0.0028i (from Petzold et al., 2009). Three dust events were observed on 16 to 22 May, 24 to 28 May, and 31 May to 5 June during the campaign. The dust age for the observations during SAMUM1 was identified to be between 0 and 2 days. In this study we collocate the average of size observations from this study as MRT class. Original data are provided as dN/dlogD in the Weinzierl et al (2009) paper and the 4−modes fitting parameters of the dust size distribution during SAMUM1 are provided in Weinzierl et al. (2011). We use here the median of the SAMUM1 data as recalculated from the lognormal parameter fitting in the Weinzierl et al. (2011) paper, their Table 5, within the diameter range 0.1 to 50 µm. The range of variability was estimated using the 3th and 97th percentile values from the logfitting curves.

- **(Müller et al., 2010):** SMPS+APS, ground−based, geometrical diameter. Size distribution observations were performed during the RHaMBLe (Reactive Halogens in the Marine Boundary Layer) campaign in May to June 2007 at Cape Verde. The particle size was measured by means of an SMPS between 0.01 and 0.9 µm, in combination with an APS measuring between 0.6 and 10 µm. To combine the particle number size distributions of the SMPS and the APS, the aerodynamic particle diameters of the APS were converted to volume equivalent diameters, as described in the paper, however details of the assumptions are not provided. Therefore we consider that the conversion factor as in Eq. (2) is 1.0 in the present analysis. The size observations were combined in the SMPS−APS overlap diameters (0.7–0.9 µm). The inlet of the measurement system was installed 4m above the ground level on the top of a measurement container used during the campaign. Size distribution for 15 May 2007 was reported and correspond to a dust−dominated case of aerosols transported from Western Africa. In our treatment we assume the APS to be the main instrument of reference for LEV2a and LEV2b corrections in both datasets. Original data are reported as number distribution in their Figure 8. Data are digitalized from the original paper, their Figure 8.

- **(Chen et al., 2011):** USHAS + APS, airborne, geometrical diameter. Aerosol size distributions during the NAMMA campaign in the Tropical Atlantic for the 0.07 to 1 µm diameter range were measured with an Ultra−High Sensitivity Aerosol Spectrometer (UHSAS) manufactured by Droplet Measurement Technologies and by means of a TSI model 3321 Aerodynamic Particle Sizer (APS) in the 0.7 to 5 µm aerodynamic diameter range. Data corresponds to dry conditions that is relative humidity (RH) less than 30%. The upper size limit of measurements indicates the inlet size cut. As discussed in the main paper, only UHSAS data up to 0.6 µm diameter were used due to instrument problems related to a reduced counting efficiency at the larger sizes during the NAMMA deployment. The UHSAS was calibrated before the campaign and also periodically during operations using latex spheres, and it was not operational for the second half of the NAMMA campaign. The APS instrument was calibrated with both latex and silicon spheres; dust particle aerodynamic diameters were converted to geometric diameters using the dynamic shape factor of 1.6 and particle mass density of 2.6 g cm^{-3}. In our treatment we assume the APS to be the main instrument of reference for LEV2a and LEV2b corrections in both datasets. Original data are reported both as dN/dlogD and dV/dlogD in their Figure 5 and error bars in the Figure represent one standard deviation estimated during the dust layer sampling period. Data are digitalized from the original paper, their Figure 5.

- **(Formenti et al., 2011):** OPC, airborne, geometrical diameter. Airborne data of dust size distribution over Niger were acquired from aircraft observations during the AMMA campaign in June−July 2006. Size distribution were obtained from an OPC (Grimm 1.108) whose measurements were corrected for the refractive index of dust by assuming a refractive index in the visible of 1.53−0.002i. The OPC was installed on an ATR−42 on the iso−axial and isokinetic AVIRAD inlet having a 50% passing efficiency at about 9 µm in diameter. The size distribution for different local erosion and Sharan transport events were reported in their Figure 10. In this paper we consider average data for V018 and V028 corresponding to local erosion event sampled with the aircraft at about 700 m asl 1−2 days

after emission and the average of V021, V022, and V036 as representative of mid−range transport conditions for dust sampled at about 2500 m asl. Data in the original paper are reported as dV/dlogD normalized to the total number concentration. Data are obtained from P. Formenti.

- **(Johnson and Osborne, 2011):** OPCs, airborne, geometrical diameter. Size distribution data for dust events over the western region of the Sahara desert were obtained during the GERBILS campaign from the UK Facility for Airborne Atmospheric Measurements (FAAM) BAe−146 aircraft. Vertical profiles acquired during ten flights showed dust layers at varying altitudes extending up to 6.5 km in the troposphere. Aerosol size distributions were measured in situ by two wing−mounted OPCs including a Passive Cavity Aerosol Spectrometer Probe (PCASP−100X) for the accumulation mode in the nominal diameter range 0.1–3.0 µm and a Small Ice Detector (SID−2) for coarse mode particles in the 2–60 µm nominal diameter range. The PCASP optical diameter was converted into a geometrical diameter by using Mie theory and a refractive index of 1.53 + 0.0015i. The SID−2 observations were corrected for the combined effects of particle shape and refractive index by applying T−matrix calculations. In our treatment we further correct these data, which already partly account for particle non sphericity, to a LEV2b dataset using an average ASR function as described in Text S4. The average of the dust distribution observations for the campaign was reported in their Figure 3 and modelled as a four modes lognormal size distribution. Original data are dN/dlogD. Data are recalculated from the logfit parameters corresponding to the dust average size in Table 2.
- **(Kandler et al., 2011):** DMS+APS+microscopy, ground−based, projected−area diameter. Measurements of the size distribution of aged dust were performed as part of the SAMUM−2 campaign in 2008, following the fresh dust characterization exercise during the SAMUM−1 campaign in 2006 (Weinzierl et al., 2009). Kandler et al. (2011) used the similar instrumentation as at the ground site of Tinfou during SAMUM−1 to measure dust size distribution at a ground station on Praia, Cape Verde in winter 2008. The aerosol size distributions in the submicron range were measured by a combination of a DMPS (mobility size range of 26–800 nm) and an APS (model 3321, TSI Inc., St. Paul, USA; aerodynamic size range of 570 nm to 10 μm). For the APS only data for particles smaller than 5 μm were used. The aerodynamic diameters were converted into volume equivalent diameters using an effective density of 2 g cm^{-3}, as documented in Schladitz et al. (2011). Particles in the size range of 4–500 μm were collected by a single−stage impactor and analysed by microscopy. The setup allowed to reduce the the size error to 3% for particles larger than 15 μm, and approximately 0.5 μm for smaller ones. The same corrections, procedure and image analysis as described by Kandler et al. (2009) were applied in Kandler et al. (2011). In our treatment we assume the microscopy to be the main reference technique for LEV2a and LEV2b correction data. Original size distributions data from three dust phases of the SAMUM2 campaign characterized by transport from the eastern Mali/western Niger area (DU2 and DU3) and southern Mauritania (shorter distance, DU1) are reported in their Figure 6 as dN/dlogD and dV/dlogD. They also report the volume size distributions for the averages of dust periods on Cape Verde and this volume distribution is used in the present study. Data are digitalized from the original paper, their Figure 6.
- **(Shao et al., 2011):** OPC, ground−based, geometrical diameter. These authors reported measurements of the vertical dust flux as observed for a strong erosion event on a flat agricultural field in Australia during the Japanese Australian Dust Experiment (JADE) in 2006. An OPC (YGK Corp. ADS−03−8CH) was used to measure the particle concentration in the 0.3–8.4 µm geometric diameter size range at 1.0, 2.0, and 3.5 m heights. Optical to geometrical diameter conversion was performed assuming a CRI of 1.5−0.001i and modeling dust as tri axis oval shape (Huang et al., 2021 supplementary information). These measurements were combined with wind speed observations to calculate the vertical dust flux as a function of friction velocity. The authors questioned the reliability of the 0.3 – 0.6 µm size bin, as discussed in Kok et al. 2017. In our treatment we further correct these data, which already partly account for particle non sphericity, to a LEV2b dataset using an average ASR function as described in Text S4. Original data are fluxes as dN m^{-2} s^{-1}. We took the treated data

from Kok et al. (2017) (average and standard deviation of the three cases in Fig. 12 from Shao et al. (2011)). Data are obtained from J. Kok (personal communication).

- **(Weinzierl et al., 2011):** OPCs, airborne, geometrical diameter. These authors report airborne observations from flights around the Cape Verde area during the SAMUM−2 campaign in 2008. Different OPCs, both wing–mounted on the DLR Falcon aircraft or inside the cabin, were used. The wing mounted had a 50% passing efficiency of 30 µm, whereas the cabin OPC sampled aerosols through an isokinetic inlet having a 50% passing efficiency at about 2.5 µm in diameter at the ground and 1.5 µm at 10 km. The visible refractive index used to correct OPC dust data was 1.55−0.003/0.004i as reported in their Table 3. Original data are reported as dN/dlogD. We use here the 4−modes fitting parameters as reported in the Weinzierl et al. (2011) paper, their Table 5, for the median of the SAMUM−2 data calculated within the diameter range 0.1 to 30 µm (upper limit of the inlet). The range of variability is estimated using the 3th and 97th percentile values from the logfitting curves

- **(Jung et al., 2013):** OPC, airborne, optical diameter. Airborne in situ measurements of dust size distribution was performed onboard Center for Interdisciplinary Remotely Piloted Aircraft Studies (CIRPAS) Twin Otter in the framework of the Barbados Aerosol Cloud Experiment (BACEX) in March−April 2010. Size distribution was measured by means of a PCASP OPC in the range of 0.1–2.5 µm. Two dust episode measurements were taken on the 1st of April within the Sahara air layer (SAL) at 2306 m, and on the 2nd of April in the SAL at 1930 m, showing very similar size distributions. We consider here the average of the datasets. Original data are shown as both number and volume distributions. Data are digitalized from the original paper, their Figure 14 c and d.

- **(Ryder et al., 2013a; 2013b):** OPC + OAP, airborne, geometrical diameter. These two papers synthetize measurements of the dust size distribution obtained during the FENNEC campaign in June 2011 over the western African desert, covering Mauritania, Mali and Canary islands, based on observations from the UK's Bae−146−301 Research Aircraft. Research flights included a total of 42 profiles acquired in an altitude range between 100 m up to around 8 km, but with most of the measurements corresponding to levels below 2−3 km. Several instruments were combined to measure the dust size distribution over a large size range, including wing−mounted PCASP 100X, CDP and CAS models OPCs, and CIP cloud probe. The measurement setup during FENNEC was in particular conceived to increase the confidence in the coarse mode size distribution measurements, in particular the coarse fraction up to 40 to 100 µm diameter, covered by different instruments simultaneously. Instrumental calibration, drift and for a refractive index of dust were accounted for in the analysis. The OPC dust data were corrected using Mie theory and assuming a real refractive index of 1.53 and an imaginary refractive index between 0.001 and 0.003 in the visible range. Data for three categories namely fresh dust, representing dust uplifted within 12 h prior observations, aged dust, for dust uplifted within 12 to 70 hours before observations, and SAL aerosols, corresponding to plumes with a mean age of 87 hours, are reported in the Ryder et al. work. In our treatment we assume the OPC data to be the main reference technique for LEV2b correction data. Original data are reported as volume size distribution. Averaged data for the three categories are obtained from C. Ryder (personal communication).

- **(Rosenberg et al., 2014):** OPC + OAP, airborne, geometrical diameter. Rosenberg et al. report measurements of the size−resolved aerosol fluxes up to 300 µm diameter as retrieved by the combination of two OPCs and an OAP using eddy covariance technique. The measurements were acquired during the FENNEC airborne campaign as described in (Ryder et al., 2013b) and refer to altitudes ranging between ~100 – 1000 m asl. Data were categorized as four different regions and at three different ranges of the vertical turbulent kinetic energy. The calibrations and the optical to geometrical diameter for OPC instruments is based on (Rosenberg et al., 2012) and assumes a refractive index of 1.53−0.001i for dust in the visible range. In our treatment, as for Ryder et al. (2013a; 2013b) we assume the OPC data to be the main reference technique for LEV2b correction data. Original data are mass and number fluxes as dN $m^{-2}\,s^{-1}$ or dM $m^{-2}\,s^{-1}$. We took the treated

data from Kok (average and standard deviation of the cases in Fig. 5 for data between 0.5 and 20 µm) to which we add the average data above 20 µm as digitalized from the original paper, their Figure 5.

- (Meloni et al., 2015). OPC, airborne, optical diameter. The measurements were taken in spring 2008 over the sea surface at the island of Lampedusa during the Ground−based and Airborne Measurements of Aerosol Radiative Forcing (GAMARF) campaign. Aircraft observations of the dust size distribution during an intense outbreak episode on the 3rd of May 2008 were obtained for dust originating in Morocco. A model 1.108 Grimm (OPC) measured the number of particles in a nominal diameter range covering the range 0.3 to 20 µm in 15 size channels. The size distribution from the Grimm measurements was integrated over the 1000 to 2000 m altitude where dust was present, and fitted with a 3−mode lognormal function. We use the 3 modes function to reproduce the dust distribution. Original data are normalized volume size distributions as shown in the original paper in their Figure S1 panel b. Data are obtained from D. Meloni (personal communication).
- (Denjean et al., 2016a). SMPS+OPC, airborne, geometrical diameter. The size distribution of dust aerosols was measured during the Dust−ATTACk field campaign that took place between 20 June and 13 July 2012 at the Cape San Juan Puerto Rico Aerosol Observatory. Instruments were installed behind a standard NOAA/ESRL/GMD aerosol inlet and measurements were performed at relative humidity below <40%. The particle number size distribution was measured by a combination of a SMPS, working in the 11.8–593.5 nm mobility diameter range, and a GRIMM 1.109 OPC, measuring within 0.25–32 µm equivalent optical diameter range. The SMPS mobility diameter was converted into a geometric diameter assuming a dry dynamic shape factor of 1.2 ± 0.09, discussed in the paper to be a good approximation for randomly oriented elongated particles. The OPC optical to geometric diameter conversion was performed assuming a refractive index of 1.53–0.002i and Mie theory for homogeneous spherical particles. Several dust events were recorded at Puerto Rico during DUST−ATTACk, with PM10 concentrations increases from 20 to 70 µg m^{-3} during the events. Main source regions were identified to localize in the Western Sahara, Mauritania, Algeria, Niger, and Mali. The volume size distributions (dV/dlogD) from SMPS and GRIMM, normalized to the total volume, for the five dust events observed during the field campaign are reported in their Figure 8. The most dust−dominated event occurred on the 3rd of July, classified as E3 (episode 3), and considered here as representative dust size distribution data for this campaign. The average and standard deviation for the size distribution data for E3 are used here. In our treatment we assume the OPC data to be the main reference technique for LEV2b correction data. Original data are normalized volume size distributions as shown in the original paper in their Figure 8. Data were obtained from C. Denjean (personal communication).
- (Denjean et al., 2016b). SMPS+OPCs, airborne, geometrical diameter. The size distribution of dust aerosols transported into the Mediterranean basin was measured during the ChArMEx/ADRIMED (the Chemistry−Aerosol Mediterranean Experiment/Aerosol Direct Radiative Impact on the regional climate in the MEDiterranean region) field campaign in June−July 2013 on board of the aircraft ATR−42. The number size distribution in the submicron range was measured with an in−cabin SMPS combined with a wing−mounted UHSAS OPC; the supermicron size was measured by two different OPCs : a wing−mounted FSSP−300 and a GRIMM 1.129. The electrical mobility diameters by the SMPS are converted into geometrical diameters assuming a dynamic shape factor of 1, therefore assuming particle sphericity. The OPCs optical diameters were converted into geometrical diameters by assuming a refractive index of 1.53 – 0.004i and homogeneous spherical particles. During ADRIMED, systematic differences in the size distributions measured by the FSSP−300 and the GRIMM were observed around 2 µm. Data between 2–10 µm and 1.5–2 µm diameter from the FSSP−300 and the GRIMM respectively were not considered in the original paper analysis. The GRIMM OPC was behind the AVIRAD inlet, having a cut−off diameter value of 12 µm as optical equivalent diameter, while the SMPS was set up behind the Community Aerosol Inlet (CAI), having a cut−off at 5 µm. The USHAS and the FSSP were wing−mounted therefore not affected by inlet cut−off limits.

Different dust episodes were encountered during the ADRIMED campaign at altitudes between 1000 and 5400 m, with dust originated between 1 and 5 days before in Tunisia, Morocco and Algeria. The average of all dust observations above 3000 m during the ADRIMED campaign, reported to be less contaminated by pollution than observations below this altitude, is considered here. The absolute variation between the maximum and the minimum of the average measured size distribution is assumed as the data uncertainty in the present analysis. In our treatment we assume the OPC data to be the main reference technique for LEV2b correction data. Original data are reported as normalized volume size distribution in their Figure 7b. Data were are digitalized from the original paper, their Figure 5.

- (Struckmeier et al., 2016). APS, ground–based, aerodynamic diameter. The size distribution was measured at Rome during the DIAPASON campaigns. Measurements were performed with an APS providing aerosol sizing between 0.5 and 20 µm aerodynamic diameter. Two DIAPASON field campaigns occurred in 2013 and 2014. Dust advection event lasting for several days was observed both years, one between 23 October and 1 November 2013, and 20 to 26 May 2014. The event in 2014 was much more intense than the one in 2013 and it is the one considered here. In 2014 dust originate at 30–35°N between Morocco (Saharan Atlas) and Tunisia (Erg Oriental). Original data are mass size distributions. Data are digitalized from the original paper, their Figure 3.
- (Weinzierl et al., 2017). OPCs, airborne, geometrical diameter. Airborne in situ aerosol size distribution measurements were obtained in the framework of the Saharan Aerosol Long–Range Transport and Aerosol–Cloud–Interaction Experiment (SALTRACE) in June 2013 with a Falcon research aircraft. A lagrangian–type study was performed during the campaign and consisted in sampling the same air mass first over Cabo Verde at the altitude of 2.6 km on 17 June 2013, and again over Barbados at 2.3 km on 22 June 2013 after its transport across the Atlantic Ocean. The aerosol total number distribution below 1 µm was retrieved by combining measurements from three Condensation Particle Counters (CPCs), and a Grimm 1.129 OPC, all instruments installed behind an isokinet inlet cutting particles at 2.5 µm diameter. Three different wing–mounted OPCs (UHSAS–A, GRIMM, FSSP) covering the nominal size range 0.06–30 µm, and a CAS–DPOL OPC measuring between 0.5 and 50 µm were set up for coarse dust sizing. Measured size data were inverted with a consistent Bayesian inversion procedure following the procedure described by (Walser et al., 2017). The full size distribution obtained was parametrized with four lognormal distributions. Original data are number size distributions as shown in Figure 9 in their paper providing a synthesis of Cabo Verde and Barbados observations. Data are digitalized from the original paper, their Figure 9.
- (Moran Zuloaga et al., 2018) OPC, ground–based data, optical diameter. Measurements were acquired in Brasil at the site of ATTO tower for the period 2014 to 2017 and contributed to the GoAmazon 2014/5 campaign. Size distribution was derived based on OPC measurements (OPS, model 3330, TSI Inc. Shoreview, MN, USA) operated continuously at the ATTO site since 30 January 2014. The OPC was set at a resolution of 5 minutes and data covered a 38 months period for the analysis presented in the original paper. The OPC instrument allowed sizing aerosols between 0.3 and 10 µm in 16 bins. It was located in a container at the base of a triangular mast sampling ambient air from a 25 mm stainless steel sampling line with a total suspended matter (TSP) inlet located at 60 m a.g.l., which corresponds to about 30 m above the canopy height. The sample air was dried to a relative humidity (RH) of about 40 %. The measured aerosol number size distributions were converted into surface and volume size distributions assuming that particles are spherical (shape factor of 1) and that their density is 1 g cm^{-3}. We consider here the volume size distribution data they reported in their Figure 6 for the advected African dust corresponding to the long range transport episodes identified (median curve as reported in their Figure 6d). In our treatment, and specifically for LEV2a data treatment, we assume that the optical to geometrical conversion is the same that the one estimated for the GRIMM 1.109 as reported in Formenti et al. (2024). As a matter of fact the physical properties of the OPS considered in this paper (operating wavelength of 660 nm and opening angle of 30 to 150°) are very similar to the GRIMM one. Original data are volume size

distributions as shown in Figure 6d in their paper. Data are taken from Table S6 in the supplement of the original paper.

- (Renard et al., 2018). OPC, airborne, optical diameter. Balloon borne observations of the dust size distribution were obtained during the ChArMEx intensive campaign in June–July 2013 in the western part of the Mediterranean basin. Measurements were performed with the LOAC OPC installed and flying on drifting boundary layer pressurised balloons (BLPBs). Different flights were performed with the LOAC during African dust plume events of the ChArMEx summer 2013 campaign. One example of measurement of the particle volume size distribution within the desert dust plume from the BLPB flight of 19 June 2013 at an altitude of 3.3 km is reported in their Figure 15. In our treatment, and specifically for LEV2b conversion, the data are left unchanged and this because of the nominal technical properties of the LOAC, measuring particle scattering in the 12° forward direction discussed by the authors to be mostly insensitive to refractive index calibration. Original data are volume size distributions as shown in Figure 15(a) in their paper. Data are digitalized from the original paper, their Figure 15.

- (Ryder et al., 2018). OPC + CIP, airborne, geometrical diameter. These authors report airborne in situ measurements of the dust size distribution as obtained in August, 2015 close to Cape Verde during the AERosol Properties –Dust (AER–D) campaign based on UK's Bae–146–301 Research Aircraft operations. The configuration was similar to the one during Fennec 2011 campaign, but in addition the AER–D campaign used cloud imaging probes (CIP15 and 2DS) for size distributions at diameters larger than 10 µm. Wing–mounted OPCs (PCASP and CDP) and shadow probes were combined to measure dust sizes between 0.1 and 100 µm diameter. The OPCs optical to geometrical diameter conversion was performed assuming Mie theory and a dust refractive index of 1.53–0.001i. The paper presents size distributions from 31 profiles and 19 in situ aerosol horizontal sampling runs. Of these, 14 horizontal runs sampled dust in the SAL at altitudes between 1.8 and 4.1 km. The age of sampled dust varied between 1 and 5 days. The AER–D mean logfit size distributions from the SAL observations reported in their Figure 6 are considered here. Original data are mean, min and max volume size distributions as shown in the original paper in their Figure 6. Data were recalculated from the lognormal fitting parameters in their Table 5 (from the corrigendum version).

- (Huang et al., 2019). OPC, ground–based, geometrical diameter. In situ field measurements of the dust size distribution at emission were acquired from a coastal sand sheet at Oceano Dunes in California from 15 May to 7 June 2015. They used six OPCs (the 212 ambient particulate profiler, manufactured by Met One Instruments, Inc.), four of which were mounted on a tower at four different heights within 0.74–6.44 m above the surface. Each OPC measured size–resolved aerosol concentrations using seven size bins with optical equivalent diameters within the range 0.49–10 µm. Of the seven size bins, only the smallest six bins with nominal diameters ranging from 0.49 to 7 µm were used, while the seventh one was removed because of reduced sampling efficiency, in particular under strong winds. The OPCs optical diameters were converted into geometric diameter using Mie calculation and a CRI of 1.53–0.003i. Normalized volume particle size distribution of dust at emission as reported in their Figure 3 and is considered in this study. Original data are volume size distributions. Data are digitalized from the original paper, their Figure 3.

- (Khalfallah et al., 2020). OPC, ground–based, geometrical diameter. Size distribution for dust erosion events were reported for observations performed during the WIND-O-V's (WIND erOsion in presence of sparse Vegetation) experiment in March to May 2017 in Tunisia, Northern Africa. Size number fluxes were measured at 2 and 4 m above ground level by means of two OPCs (PALAS Welas). Each OPC was equipped with an omnidirectional total suspended particles (TSP) sampling head for which the collection efficiency varied with wind speed and ranged from 79% at 0.56 m/s to 99% at 2.2 m/s, and 102% at 6.7 m/s for a mass median diameter of 15 µm. Because the range of wind velocity measured during the emission periods was >5 m/s at about 2 m, it is expected that no significant loss of coarse particles occurred. The optical to geometrical diameter conversion was performed by Mie theory assuming a refractive index of 1.43–0i, considered a value representative for silica. The OPCs

measured the size distributions of the vertical number dust flux for 8 dust emission events lasting for 5 to 9 hours each. Original data are reported as the average of the size distribution over the duration of each event in their Figure 5 as dN cm^{-2} s^{-1}. The average and standard deviation of the size obtained for the eight events is considered in the present study. Data are digitalized from the original paper, their Figure 5.

- **(González–Flórez et al., 2023)**. OPC, ground–based, geometrical diameter. Size distribution for dust erosion events were reported for observations performed at the ground during a field campaign in the Moroccan Sahara in September 2019. The campaign was in the context of the FRontiers in dust minerAloGical coMposition and its Effects upoN climaTe (FRAGMENT) project. Size number fluxes were measured at 1.8 and 3.5 m above ground level by means of two OPCs (Fidas 200S, Palas GmbH) sampling from a Sigma–2 head (Palas GmbH). The sampling efficiency of the sampling head was not measured, but the authors indicate that it is insensitive to wind speed up to 6ms^{-1} in the PM10 range by previous studies. The used OPC sizes particles in 63 size bins (equally–spaced in logarithmic scale) in a nominal diameter range of 0.2 to 19.1 µm. Data from the first three bins of the OPCs (< 0.25 µm) were discarded because reported to show unrealistic behaviour. The measured number particle concentrations were averaged over 15 min and classified over different intervals of friction velocity. The optical to geometrical diameter conversion of the OPCs diameters was performed assuming ellipsoidal dust particles based on a database of shape–resolved single scattering properties as in Huang et al. (2021). For initializing the calculations an aspect ratio (AR) of 1.46 is assumed, at the median of the measurements during the campaign based on microscopy analysis, while the height–to–width ratio (HWR) is set at 0.45 µm. A refractive index of 1.49–0.0015i is assumed for Moroccan dust. Emission size distribution data are reported in the paper as averages over different classes of friction velocity and for well–developed erosion conditions during regular events and for two haboob events. In this study we consider the size distribution for regular events corresponding to friction velocity range of 0.30 to 0.35 m s^{-1} (at the middle of their investigated range) as representative of the campaign data. To note that data from this study within the range 11.25–17.83 µm are not taken into account for LEV2b mean calculations presented in Fig. 2 and 3 for the SOURCE category in the main as they strongly biased the mean size in this specific range. They are taken into account in the standard deviation calculation. Original data are reported as the average normalized emission flux size distribution for well–developed erosion conditions during regular events in their Figure 13 (panel e). The size obtained for the average friction velocity range of 0.30–0.35 m s^{-1} is considered in the present study. Data are digitalized from the original paper, their Figure 13.

Supplementary references

d'Almeida, G. A.: On the variability of desert aerosol radiative characteristics, J. Geophys. Res: Atmos., 92, 3017–3026, https://doi.org/10.1029/JD092iD03p03017, 1987.

d'Almeida, G. A. and Schütz, L.: Number, Mass and Volume Distributions of Mineral Aerosol and Soils of the Sahara, J. Climate Appl. Meteor., 22, 233–243, https://doi.org/10.1175/1520–0450(1983)022<0233:NMAVDO>2.0.CO;2, 1983.

Basart, S., Pérez, C., Cuevas, E., Baldasano, J. M., and Gobbi, G. P.: Aerosol characterization in Northern Africa, Northeastern Atlantic, Mediterranean Basin and Middle East from direct–sun AERONET observations, Atmos. Chem. Phys., 9, 8265–8282, https://doi.org/10.5194/acp–9–8265–2009, 2009.

Bates, T. S., Coffman, D. J., Covert, D. S., and Quinn, P. K.: Regional marine boundary layer aerosol size distributions in the Indian, Atlantic, and Pacific Oceans: A comparison of INDOEX measurements with ACE–1, ACE–2, and Aerosols99, J. Geophys. Res., 107, INX2 25–1–INX2 25–15, https://doi.org/10.1029/2001JD001174, 2002.

Chen, G., Ziemba, L. D., Chu, D. A., Thornhill, K. L., Schuster, G. L., Winstead, E. L., Diskin, G. S., Ferrare, R. A., Burton, S. P., Ismail, S., Kooi, S. A., Omar, A. H., Slusher, D. L., Kleb, M. M., Reid, J. S., Twohy, C. H., Zhang, H., and Anderson, B. E.: Observations of Saharan dust microphysical and optical properties from the Eastern Atlantic during NAMMA airborne field campaign, Atmos. Chem. Phys., 11, 723–740, https://doi.org/10.5194/acp–11–723–2011, 2011.

Chou, C., Formenti, P., Maille, M., Ausset, P., Helas, G., Harrison, M., and Osborne, S.: Size distribution, shape, and composition of mineral dust aerosols collected during the African Monsoon Multidisciplinary Analysis Special Observation Period 0: Dust and Biomass–Burning Experiment field campaign in Niger, January 2006, J. Geophys. Res., 113, https://doi.org/10.1029/2008JD009897, 2008.

Clarke, A. D., Shinozuka, Y., Kapustin, V. N., Howell, S., Huebert, B., Doherty, S., Anderson, T., Covert, D., Anderson, J., Hua, X., Moore, K. G., McNaughton, C., Carmichael, G., and Weber, R.: Size distributions and mixtures of dust and black carbon aerosol in Asian outflow: Physiochemistry and optical properties, J. Geophys. Res., 109, https://doi.org/10.1029/2003JD004378, 2004.

De Carlo, P.F., Jay G. Slowik, Douglas R. Worsnop, Paul Davidovits & Jose L. Jimenez (2004) Particle Morphology and Density Characterization by Combined Mobility and Aerodynamic Diameter Measurements. Part 1: Theory, Aeros. Sci. Tech., 38:12, 1185–1205, DOI: 10.1080/027868290903907.

Denjean, C., Formenti, P., Desboeufs, K., Chevaillier, S., Triquet, S., Maillé, M., Cazaunau, M., Laurent, B., Mayol-Bracero, O. L., Vallejo, P., Quiñones, M., Gutierrez-Molina, I. E., Cassola, F., Prati, P., Andrews, E., and Ogren, J.: Size distribution and optical properties of African mineral dust after intercontinental transport, J. Geophys. Res., 121, 7117–7138, https://doi.org/10.1002/2016JD024783, 2016a.

Denjean, C., Cassola, F., Mazzino, A., Triquet, S., Chevaillier, S., Grand, N., Bourrianne, T., Momboisse, G., Sellegri, K., Schwarzenbock, A., Freney, E., Mallet, M., and Formenti, P.: Size distribution and optical properties of mineral dust aerosols transported in the western Mediterranean, Atmos. Chem. Phys., 16, 1081–1104, https://doi.org/10.5194/acp–16–1081–2016, 2016b.

Dubovik, O., and King, M. D.: A flexible inversion algorithm for retrieval of aerosol optical properties from Sun and sky radiance measurements, J. Geophys. Res., 105, 20673–20696, https://doi.org/10.1029/2000JD900282, 2000.

Dubovik, O., Sinyuk, A., Lapyonok, T., Holben, B. N., Mishchenko, M., Yang, P., Eck, T. F., Volten, H., Muñoz, O., Veihelmann, B., van der Zande, W. J., Leon, J.–F., Sorokin, M., and Slutsker, I.: Application of spheroid models to account for aerosol particle non sphericity in remote sensing of desert dust, J. Geophys. Res., 111, D11208, https://doi.org/10.1029/2005JD006619, 2006.

Formenti, P., Andreae, M. O., Lange, L., Roberts, G., Cafmeyer, J., Rajta, I., Maenhaut, W., Holben, B. N., Artaxo, P., and Lelieveld, J.: Saharan dust in Brazil and Suriname during the Large–Scale Biosphere–Atmosphere Experiment in Amazonia (LBA) – Cooperative LBA Regional Experiment (CLAIRE) in March 1998, J. Geophys. Res., 106, 14919–14934, https://doi.org/10.1029/2000JD900827, 2001.

Formenti, P., Rajot, J. L., Desboeufs, K., Saïd, F., Grand, N., Chevaillier, S., and Schmechtig, C.: Airborne observations of mineral dust over western Africa in the summer Monsoon season: spatial and vertical variability of physico–chemical and optical properties, Atmos. Chem. Phys., 11, 6387–6410, https://doi.org/10.5194/acp–11–6387–2011, 2011.

Formenti, P., Di Biagio, C., Huang, Y., Kok, J., Mallet, M. D., Boulanger, D., and Cazaunau, M.: Look–up tables resolved by complex refractive index to correct particle sizes measured by common research–grade optical particle counters, Atmos. Meas. Tech. Discuss. [preprint], https://doi.org/10.5194/amt–2021–403, in review, 2021.

Fratini, G., Ciccioli, P., Febo, A., Forgione, A., and Valentini, R.: Size–segregated fluxes of mineral dust from a desert area of northern China by eddy covariance, Atmos. Chem. Phys., 7, 2839–2854, https://doi.org/10.5194/acp–7–2839–2007, 2007.

Gillette, D. A., Blifford, I. H., and Fenster, C. R.: Measurements of Aerosol Size Distributions and Vertical Fluxes of Aerosols on Land Subject to Wind Erosion, J. Appl. Meteor., 11, 977–987, https://doi.org/10.1175/1520–0450(1972)011<0977:MOASDA>2.0.CO;2, 1972.

Gillette, D.A. On the production of soil wind erosion having the potential for long range transport. J. Rech. Atmos. 8, 734–744 (1974).

Gillette, D. A., Blifford, I. H., and Fryrear, D. W.: The influence of wind velocity on the size distributions of aerosols generated by the wind erosion of soils, J. Geophys. Res. 79, 4068–4075, https://doi.org/10.1029/JC079i027p04068, 1974.

Gillette, D. A. and Nagamoto, C. 1993. Size distribution and single particle composition for two dust storms in Soviet central Asia in September 1989 and size distribution and chemical composition of local soil. In: Joint Soviet–American Experiment on Arid Aerosol (eds. G. S. Golitsyn, D. A. Gillette, T. Johnson, V. N. Ivanov, S. M. Kolomiyets, and co–editors). Hydrometeoizdat, St. Petersburg, 135–146.

González–Flórez, C., Klose, M., Alastuey, A., Dupont, S., Escribano, J., Etyemezian, V., Gonzalez–Romero, A., Huang, Y., Kandler, K., Nikolich, G., Panta, A., Querol, X., Reche, C., Yus–Díez, J., and Pérez García–Pando, C.: Insights into the size–resolved dust emission from field measurements in the Moroccan Sahara, Atmos. Chem. Phys., 23, 7177–7212, https://doi.org/10.5194/acp–23–7177–2023, 2023.

Hinds, W. C.: Aerosol technology: properties, behavior, and measurement of airborne particles, John Wiley & Sons, Chichester, 504 pp., 1999.

Huang, Y., Kok, J. F., Martin, R. L., Swet, N., Katra, I., Gill, T. E., Reynolds, R. L., and Freire, L. S.: Fine dust emissions from active sands at coastal Oceano Dunes, California, Atmos. Chem. Phys., 19, 2947–2964, https://doi.org/10.5194/acp–19–2947–2019, 2019.

Huang, Y., Adebiyi, A. A., Formenti, P., & Kok, J. F. (2021). Linking the different diameter types of aspherical desert dust indicates that models underestimate coarse dust emission. Geophys. Res. Lett., 48, e2020GL092054. https://doi.org/10.1029/2020GL092054

Huang, Y., Kok, J. F., Kandler, K., Lindqvist, H., Nousiainen, T., Sakai, T., et al. (2020). Climate models and remote sensing retrievals neglect substantial desert dust asphericity. Geophys. Res. Lett., 47, e2019GL086592. https://doi.org/10.1029/2019GL086592

Johnson, B. T. and Osborne, S. R.: Physical and optical properties of mineral dust aerosol measured by aircraft during the GERBILS campaign, Q. J. Royal Met. Soc.137, 1117–1130, https://doi.org/10.1002/qj.777, 2011.

Jung, E., Albrecht, B., Prospero, J. M., Jonsson, H. H., and Kreidenweis, S. M.: Vertical structure of aerosols, temperature, and moisture associated with an intense African dust event observed over the eastern Caribbean, J. Geophys. Res., 118, 4623–4643, https://doi.org/10.1002/jgrd.50352, 2013.

Kandler, K., Benker, N., Bundke, U., Cuevas, E., Ebert, M., Knippertz, P., Rodriguez, S., Schütz, L., and Weinbruch, S.: Chemical composition and complex refractive index of Saharan mineral dust at Izana, Tenerife (Spain) derived by electron microscopy, Atmos. Environ., 41, 8058–8074, 2007.

Kandler, K., Schütz, L., Deutscher, C., Ebert, M., Hofmann, H., JäCKEL, S., Jaenicke, R., Knippertz, P., Lieke, K., Massling, A., Petzold, A., Schladitz, A., Weinzierl, B., Wiedensohler, A., Zorn, S., and Weinbruch1, S.: Size distribution, mass concentration, chemical and mineralogical composition and derived optical parameters of the boundary layer aerosol at Tinfou, Morocco, during SAMUM 2006, Tellus B., 61, 32–50, https://doi.org/10.1111/j.1600–0889.2008.00385.x, 2009.

Kandler, K., Schütz, L., Jäckel, S., Lieke, K., Emmel, C., Müller–Ebert, D., Ebert, M., Scheuvens, D., Schladitz, A., Šegvić, B., Wiedensohler, A., and Weinbruch, S.: Ground–based off–line aerosol measurements at Praia, Cape

Verde, during the Saharan Mineral Dust Experiment: microphysical properties and mineralogy, Tellus B., 63, 459–474, https://doi.org/10.1111/j.1600–0889.2011.00546.x, 2011.

Khalfallah, B., Bouet, C., Labiadh, M. T., Alfaro, S. C., Bergametti, G., Marticorena, B., Lafon, S., Chevaillier, S., Féron, A., Hease, P., Tureaux, T. H. des, Sekrafi, S., Zapf, P., and Rajot, J. L.: Influence of Atmospheric Stability on the Size Distribution of the Vertical Dust Flux Measured in Eroding Conditions Over a Flat Bare Sandy Field, J. Geophys. Res., 125, e2019JD031185, https://doi.org/10.1029/2019JD031185, 2020.

Kobayashi, H., Arao, K., Murayama, T., Iokibe, K., Koga, R., and Shiobara, M.: High–Resolution Measurement of Size Distributions of Asian Dust Using a Coulter Multisizer, J. Atmos. Oceanic Technol., 24, 194–205, https://doi.org/10.1175/JTECH1965.1, 2007.

Kok, J. F., Ridley, D. A., Zhou, Q., Miller, R. L., Zhao, C., Heald, C. L., Ward, D. S., Albani, S., and Haustein, K.: Smaller desert dust cooling effect estimated from analysis of dust size and abundance, Nat. Geo., 10, 274–278, https://doi.org/10.1038/ngeo2912, 2017.

Mahowald, N., Albani, S., Kok, J. F., Engelstaeder, S., Scanza, R., Ward, D. S., and Flanner, M. G.: The size distribution of desert dust aerosols and its impact on the Earth system, Aeol. Res., 15, 53–71, doi:10.1016/j.aeolia.2013.09.002, 2014

Maring, H., Savoie, D. L., Izaguirre, M. A., McCormick, C., Arimoto, R., Prospero, J. M., and Pilinis, C.: Aerosol physical and optical properties and their relationship to aerosol composition in the free troposphere at Izaña, Tenerife, Canary Islands, during July 1995, J. Geophys. Res., 105, 14677–14700, https://doi.org/10.1029/2000JD900106, 2000.

Maring, H., Savoie, D. L., Izaguirre, M. A., Custals, L., and Reid, J. S.: Mineral dust aerosol size distribution change during atmospheric transport, J. Geophys. Res., 108, https://doi.org/10.1029/2002JD002536, 2003.

McConnell, C. L., Highwood, E. J., Coe, H., Formenti, P., Anderson, B., Osborne, S., Nava, S., Desboeufs, K., Chen, G., and Harrison, M. a. J.: Seasonal variations of the physical and optical characteristics of Saharan dust: Results from the Dust Outflow and Deposition to the Ocean (DODO) experiment, J. Geophys. Res., 113, https://doi.org/10.1029/2007JD009606, 2008.

Meloni, D., Junkermann, W., Sarra, A. di, Cacciani, M., Silvestri, L. D., Iorio, T. D., Estellés, V., Gómez-Amo, J. L., Pace, G., and Sferlazzo, D. M.: Altitude–resolved shortwave and longwave radiative effects of desert dust in the Mediterranean during the GAMARF campaign: Indications of a net daily cooling in the dust layer, J. Geophys. Res., 120, 3386–3407, https://doi.org/10.1002/2014JD022312, 2015.

Mishchenko, M. I., Travis, L. D., Kahn, R. A., and West, R. A.: Modeling phase function for dustlike tropospheric aerosols using a shape mixture of randomly oriented poly–disperse spheroids, J. Geophys. Res., 102, 16831–16847, https://doi.org/10.1029/96JD02110, 1997.

Müller, K., Lehmann, S., van Pinxteren, D., Gnauk, T., Niedermeier, N., Wiedensohler, A., and Herrmann, H.: Particle characterization at the Cape Verde atmospheric observatory during the 2007 RHaMBLe intensive, Atmos. Chem. Phys., 10, 2709–2721, https://doi.org/10.5194/acp–10–2709–2010, 2010.

Osborne, S. R., Johnson, B. T., Haywood, J. M., Baran, A. J., Harrison, M. a. J., and McConnell, C. L.: Physical and optical properties of mineral dust aerosol during the Dust and Biomass–burning Experiment, J. Geophys. Res., 113, https://doi.org/10.1029/2007JD009551, 2008.

Otto, S., de Reus, M., Trautmann, T., Thomas, A., Wendisch, M., and Borrmann, S.: Atmospheric radiative effects of an in situ measured Saharan dust plume and the role of large particles, Atmos. Chem. Phys. 7, 4887–4903, https://doi.org/10.5194/acp–7–4887–2007, 2007.

Quinn, P. K., Coffman, D. J., Bates, T. S., Miller, T. L., Johnson, J. E., Welton, E. J., Neusüss, C., Miller, M., and Sheridan, P. J., Aerosol optical properties during INDOEX 1999: Means, variability, and controlling factors, J. Geophys. Res., 107, 8020, doi:10.1029/2000JD000037, 2002.

Rajot, J. L., Formenti, P., Alfaro, S., Desboeufs, K., Chevaillier, S., Chatenet, B., Gaudichet, A., Journet, E., Marticorena, B., Triquet, S., Maman, A., Mouget, N., and Zakou, A.: AMMA dust experiment: An overview of measurements performed during the dry season special observation period (SOP0) at the Banizoumbou (Niger) supersite, J. Geophys. Res., 113, https://doi.org/10.1029/2008JD009906, 2008.

Reid, E. A., Reid, J. S., Meier, M. M., Dunlap, M. R., Cliff, S. S., Broumas, A., Perry, K., and Maring, H.: Characterization of African dust transported to Puerto Rico by individual particle and size segregated bulk analysis, J. Geophys. Res., 108, https://doi.org/10.1029/2002JD002935, 2003a.

Reid, J. S., Jonsson, H. H., Maring, H. B., Smirnov, A., Savoie, D. L., Cliff, S. S., Reid, E. A., Livingston, J. M., Meier, M. M., Dubovik, O., and Tsay, S.–C.: Comparison of size and morphological measurements of coarse mode dust particles from Africa, J. Geophys. Res., 108, https://doi.org/10.1029/2002JD002485, 2003b.

Reid, J. S., Reid, E. A., Walker, A., Piketh, S., Cliff, S., Mandoos, A. A., Tsay, S.–C., and Eck, T. F.: Dynamics of southwest Asian dust particle size characteristics with implications for global dust research, J. Geophys. Res., 113, https://doi.org/10.1029/2007JD009752, 2008.

Renard, J.–B., Dulac, F., Durand, P., Bourgeois, Q., Denjean, C., Vignelles, D., Couté, B., Jeannot, M., Verdier, N., and Mallet, M.: In situ measurements of desert dust particles above the western Mediterranean Sea with the balloon–borne Light Optical Aerosol Counter/sizer (LOAC) during the ChArMEx campaign of summer 2013, Atmos. Chem. Phys., 18, 3677–3699, https://doi.org/10.5194/acp–18–3677–2018, 2018.

de Reus, M., Dentener, F., Thomas, A., Borrmann, S., Ström, J., and Lelieveld, J.: Airborne observations of dust aerosol over the North Atlantic Ocean during ACE 2: Indications for heterogeneous ozone destruction, J. Geophys. Res., 105, 15263–15275, https://doi.org/10.1029/2000JD900164, 2000.

Rosenberg, P. D., Dean, A. R., Williams, P. I., Dorsey, J. R., Minikin, A., Pickering, M. A., and Petzold, A.: Particle sizing calibration with refractive index correction for light scattering optical particle counters and impacts upon PCASP and CDP data collected during the Fennec campaign, Atmos. Meas. Tech., 5, 1147–1163, https://doi.org/10.5194/amt–5–1147–2012, 2012.

Rosenberg, P. D., Parker, D. J., Ryder, C. L., Marsham, J. H., Garcia-Carreras, L., Dorsey, J. R., Brooks, I. M., Dean, A. R., Crosier, J., McQuaid, J. B., and Washington, R.: Quantifying particle size and turbulent scale dependence of dust flux in the Sahara using aircraft measurements, J. Geophys. Res., 119, 7577–7598, https://doi.org/10.1002/2013JD021255, 2014.

Ryder, C. L., Highwood, E. J., Lai, T. M., Sodemann, H., and Marsham, J. H.: Impact of atmospheric transport on the evolution of microphysical and optical properties of Saharan dust, Geophys. Res. Lett., 40, 2433–2438, https://doi.org/10.1002/grl.50482, 2013a.

Ryder, C. L., Highwood, E. J., Rosenberg, P. D., Trembath, J., Brooke, J. K., Bart, M., Dean, A., Crosier, J., Dorsey, J., Brindley, H., Banks, J., Marsham, J. H., McQuaid, J. B., Sodemann, H., and Washington, R.: Optical properties of Saharan dust aerosol and contribution from the coarse mode as measured during the Fennec 2011 aircraft campaign, Atmos. Chem. Phys., 13, 303–325, https://doi.org/10.5194/acp–13–303–2013, 2013b.

Ryder, C. L., Marenco, F., Brooke, J. K., Estelles, V., Cotton, R., Formenti, P., McQuaid, J. B., Price, H. C., Liu, D., Ausset, P., Rosenberg, P. D., Taylor, J. W., Choularton, T., Bower, K., Coe, H., Gallagher, M., Crosier, J., Lloyd, G., Highwood, E. J., and Murray, B. J.: Coarse–mode mineral dust size distributions, composition and optical properties from AER–D aircraft measurements over the tropical eastern Atlantic, Atmos. Chem. Phys., 18, 17225–17257, https://doi.org/10.5194/acp–18–17225–2018, 2018.

Sanchez–Marroquin, A., Hedges, D. H. P., Hiscock, M., Parker, S. T., Rosenberg, P. D., Trembath, J., Walshaw, R., Burke, I. T., McQuaid, J. B., and Murray, B. J.: Characterisation of the filter inlet system on the FAAM BAe–146 research aircraft and its use for size–resolved aerosol composition measurements, Atmos. Meas. Tech., 12, 5741–5763, https://doi.org/10.5194/amt–12–5741–2019, 2019.

Schladitz, A., Müller, T., Nowak, A., Kandler, K., Lieke, K., Massling, A., and Wiedensohler, A.: In situ aerosol characterization at Cape Verde, Tellus B, 63, 531–548, https://doi.org/10.1111/j.1600–0889.2011.00569.x, 2011.

Schütz, L. and Jaenicke, R.: Particle Number and Mass Distributions above 10–4 cm Radius in Sand and Aerosol of the Sahara Desert, J. Appl. Meteor., 13, 863–870, https://doi.org/10.1175/1520–0450(1974)013<0863:PNAMDA>2.0.CO;2, 1974.

Schütz, L., Jaenicke, R. and Pietrek, H., Saharan Dust Transport over the North Atlantic Ocean. In: Péwé, T.L., Ed., Desert Dust, Geological Society of America, Boulder, Special Paper, Vol. 186, 87-100. https://doi.org/10.1130/SPE186-p87, 1981.

Shao, Y., Ishizuka, M., Mikami, M., and Leys, J. F.: Parameterization of size–resolved dust emission and validation with measurements, J. Geophys. Res., 116, https://doi.org/10.1029/2010JD014527, 2011.

Sow, M., Alfaro, S. C., Rajot, J. L., and Marticorena, B.: Size resolved dust emission fluxes measured in Niger during 3 dust storms of the AMMA experiment, Atmos. Chem. Phys., 9, 3881–3891, https://doi.org/10.5194/acp–9–3881–2009, 2009.

Struckmeier, C., Drewnick, F., Fachinger, F., Gobbi, G. P., and Borrmann, S.: Atmospheric aerosols in Rome, Italy: sources, dynamics and spatial variations during two seasons, Atmos. Chem. Phys., 16, 15277–15299, https://doi.org/10.5194/acp–16–15277–2016, 2016.

Sviridenkov, M. A., Gillette, D. A., Isakov, A. A., Sokolik, I. N., Smirnov, V. V., Belan, B. D., Pachenko, M. V., Andronova, A. V., Kolomiets, S. M., Zhukov, V. M., and Zhukovsky, D. A.: Size distributions of dust aerosol measured during the Soviet–American experiment in Tadzhikistan, 1989, Atmos. Environ., 27, 2481–2486, https://doi.org/10.1016/0960–1686(93)90019–U, 1993.

Wagner, F., Bortoli, D., Pereira, S., Costa, M. Jo., Silva, A. M., Weinzierl, B., Esselborn, M., Petzold, A., Rasp, K., Heinold, B., and Tegen, I.: Properties of dust aerosol particles transported to Portugal from the Sahara desert, Tellus B, 61, 297–306, https://doi.org/10.1111/j.1600–0889.2008.00393.x, 2009.

Walser, A., Sauer, D., Spanu, A., Gasteiger, J., and Weinzierl, B.: On the parametrization of optical particle counter response including instrument–induced broadening of size spectra and a self–consistent evaluation of calibration measurements, Atmos. Meas. Tech., 10, 4341–4361, https://doi.org/10.5194/amt–10–4341–2017, 2017.

Wendisch, M., and J.–L. Brenguier, Airborne Measurements for Environmental Research, Wiley–VCH., 2013

Weinzierl, B., Petzold, A., Esselborn, M., Wirth, M., Rasp, K., Kandler, K., Schütz, L., Koepke, P., and Fiebig, M.: Airborne measurements of dust layer properties, particle size distribution and mixing state of Saharan dust during SAMUM 2006, Tellus B, 61, 96–117, https://doi.org/10.1111/j.1600–0889.2008.00392.x, 2009.

Weinzierl, B., Sauer, D., Esselborn, M., Petzold, A., Veira, A., Rose, M., Mund, S., Wirth, M., Ansmann, A., Tesche, M., Gross, S., and Freudenthaler, V.: Microphysical and optical properties of dust and tropical biomass burning aerosol layers in the Cape Verde region—an overview of the airborne in situ and lidar measurements during SAMUM–2, Tellus B, 63, 589–618, https://doi.org/10.1111/j.1600–0889.2011.00566.x, 2011.

Weinzierl, B., Ansmann, A., Prospero, J. M., Althausen, D., Benker, N., Chouza, F., Dollner, M., Farrell, D., Fomba, W. K., Freudenthaler, V., Gasteiger, J., Groß, S., Haarig, M., Heinold, B., Kandler, K., Kristensen, T. B., Mayol–Bracero, O. L., Müller, T., Reitebuch, O., Sauer, D., Schäfler, A., Schepanski, K., Spanu, A., Tegen, I., Toledano, C., and Walser, A.: The Saharan Aerosol Long–Range Transport and Aerosol–Cloud–Interaction Experiment: Overview and Selected Highlights, Bull. Amer. Meteor. Soc., 98, 1427–1451, https://doi.org/10.1175/BAMS–D–15–00142.1, 2017.